Lane Change Path Planning

With state-dependent safety constraints using Nonlinear Model Predictive Control

C.D. Berger

Master of Science Thesis

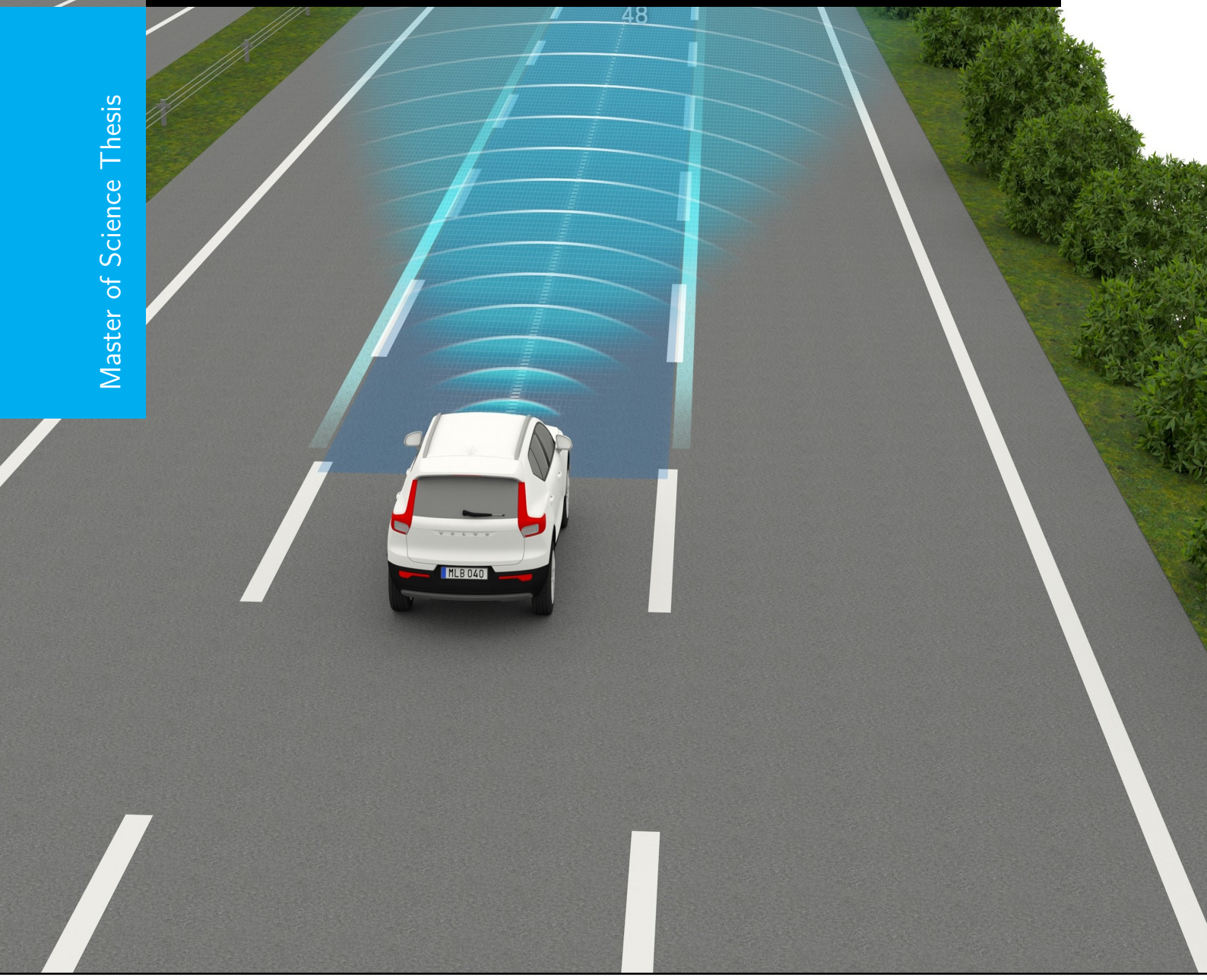

TU Delft Delft University of Technology

Delft Center for Systems and Control

Lane Change Path Planning

With state-dependent safety constraints using Nonlinear Model Predictive Control

Master of Science Thesis

For the degree of Master of Science in Systems and Control at Delft University of Technology

C.D. Berger

February 12, 2018

Faculty of Mechanical, Maritime and Materials Engineering (3mE) · Delft University of Technology

The work in this thesis was supported by Volvo Car Corporation and Zenuity in Gothenburg. Their cooperation is hereby gratefully acknowledged.

Copyright © Delft Center for Systems and Control (DCSC)
All rights reserved.

Abstract

In the past years a number of SAE level 2 driving automation systems have come available in commercial vehicles. An example is Volvo's Pilot Assist, which provides a more comfortable journey for the driver as certain parts of the dynamic driving task are taken away, but it still requires the driver to be attentive in order to supervise the system and resume vehicle operation if necessary. Car manufacturers and high-tech companies all around the world are working on the development of an Automated Driving System (ADS) of level 3 or higher where the driver does not need to supervise, but have so far not been able to introduce any to the public. Operating a vehicle on an empty highway is relatively easy, but roads are getting more and more congested so dense traffic driving needs to be accounted for as well.

One of the issues is that unsupervised driving does not only require that a system itself operates the vehicle correctly, but requires that it is able to cope with mistakes of other drivers. In order to take these into account as well as other unpredictable events, current driving automation systems tend to adopt large longitudinal margins with respect to surrounding traffic to use their ability to brake to avoid a collision. In dense traffic situations this conservative behaviour prohibits the ADS from making lane changes. This thesis was setup in cooperation with Volvo Cars / Zenuity to develop a lane change path planning algorithm that can plan *active* lane changes in dense traffic, by pushing into a gap without compromising the ability to avoid a possible collision.

Earlier work at Volvo suggested considering the ability of a vehicle to not only brake, but also to make an evasive maneuver. If an evasion maneuver is available the necessary safety margins are reduced considerably compared to a 'braking-only' scenario.

In this work, the evasive maneuver was modeled and a constraint formulation was developed that if met, guarantees the availability of the designed evasion maneuver. This constraint translates to a state-dependent safety zone which the ADS should keep the vehicle clear off at all times.

Model Predictive Control allows the implementation of such a safety zone by considering it as a constraint on the optimisation, guaranteeing that an evasion maneuver is available along any point on the prediction horizon. This negates the necessity to plan all possible evasion maneuvers separately, and it was therefore chosen as the path planning method.

Implementation of the safety zone constraint on multiple surrounding vehicles, spread over multiple lanes in a Model Predictive Control framework, together with the requirements of being able to overtake other vehicles within the prediction horizon, necessitated the development of a novel 3-step algorithm. In this algorithm three Optimal Control Problems are solved

consecutively to plan a path which positions the ego-vehicle optimally in the targeted gap without breaching the safety zones.

To be able to implement the algorithm in real-time, a computationally expedient vehicle model is chosen and the OCP's are solved using state-of-the-art structure exploiting Interior Point solvers, generated as efficient C-code using FORCES Pro.

With this setup, computation times of ∼30[ms] are achieved for a 10[s] prediction horizon sampled at 100[ms]. The algorithm is demonstrated in simulation and shown to be able to find the point of maximum lateral intrusion, to operate on the edge of the safety zone constraint, and to avoid a collision when it is being cut off from behind or when the vehicle in front comes to a sudden stop.

The results show that vehicle operation by an ADS is possible in dense traffic without compromising safety. By using the developed safety zones and novelty solution framework the necessary margins can be reduced, increasing the availability of the lane change maneuver. Furthermore the control strategies necessary for implementation are shown to be applicable in real-time, paving the way for implementation in real vehicles. This way the research contributes to the next step in developing a usable Automated Driving System.

Table of Contents

List of Figures

List of Tables

Preface

On the 12th of November 2015, one of Google's self-driving vehicles was pulled over by the police in Mountain View, California. It was not speeding, nor did it run a red light. The officer pulled the vehicle over because it was driving too slow. Almost exactly half a year later, on May 7th 2016, Joshua Brown was killed because his Tesla Model S drove into a white truck-trailer combination missed by the object detection software.

These two incidents high-light strikingly the dillemas brought up in the development of Automated Driving Systems. The system can either be designed to act very conservatively in order to guarantee occupant safety, or it can be designed to be usable in every day traffic but run the risk of getting into an accident. Volvo plans to have no-one killed or seriously injured in a new Volvo by 2020, and to have it's first level 3 ADS-equipped vehicle on the market in 2021, so it is imperative that these dilemmas are solved. This thesis aims at tackling part of this problem by by combining human-like behaviour which seems risky at first glance, with the conservativeness of having a back-up maneuver available at all times, so the occupant never runs any risk. Safe *and* usable, and hopefully a step towards true autonomy.

Acknowledgements

First and foremost I would like to thank the members of the Precautionary Safety and Collision Avoidance groups within Zenuity. From the first day I started in Volvo until the day I left Zenuity they made me feel welcome and at home, and like a true colleague.

In particular I would like to thank Mattias Brännstrom, for the fruitful discussions we had and for always taking the time to sit down with me, but also for being a friend outside work. I would like to thank Roozbeh Kianfar for introducing me to Volvo, and for his guidance in keeping me on target and on schedule.

I would like to thank my supervisors in Delft, Tamas Keviczky and Barys Shyrokau for their assistance in writing this thesis. Tamas deserves my appreciation for his patience whilst I was in Sweden and for allowing me to pursue my course of research. I want to thank Barys for his advice and for always being available for discussions through his own busy schedule, even in the evenings and weekends.

Lastly I would like to thank Donna for her love and dedication in supporting my move to Sweden, even if it meant being apart for 9 months.

Delft, University of Technology C.D. Berger
February 12, 2018

Chapter 1

Introduction

As of 2017, many of the major car manufacturers are working on systems bringing various levels of driving automation systems to their vehicles. While Advanced Driver Assistance Systems (ADAS) such as Adaptive Cruise Control (ACC) and Lane Keeping Aid (LKA) are becoming increasingly common on the road they still require active driver supervision. The next outlook is increased levels of autonomy that allow the driver to be more withdrawn from the driving task.

Human drivers make mistakes, but also anticipate mistakes of other drivers. They drive in such a way that they can cope with these mistakes and, to a certain level, react to unforeseen events on the roads, such as sudden hard braking or accidents.

If Automated Driving Systems (ADS), defined as driving automation systems of SAE level 3 or higher[4], are to reach any significant level of user-acceptance they need to be at least as safe, but most probably a lot safer than human drivers[5]. That means they should not only not make mistakes themselves, but also be extremely robust to actions of other road-users and potential incidents. Current driving automation systems achieve this by incorporating large safety margins, but this limits their ability to smoothly navigate through traffic. Especially in dense traffic situations where inter-vehicle gaps become prohibitively small the systems ability to make lane changes is severely limited. If this very conservative driving behaviour is transferred to level 3 systems, in can negatively affect the adoption rate.

To aid the adoption of higher level systems, the ADS will thus need to be able to mimic the human squeeze-in behaviour in dense traffic, but in a safe way. This thesis aims at tackling that problem by developing a lane change path planning algorithm that minimizes the safety margins that have to be taken into account, and can at the same time still provide guarantees regarding safety. The following sections will explain the motivation behind the solution, the writer's specific contribution to it and finally the structure of this thesis report.

1-1 Motivation

Currently, Automated Driving Systems in development at Volvo/Zenuity attempt to provide guarantees regarding safety by incorporating large longitudinal margins to be able to use the vehicle's braking abilities to account for unexpected events.

When the inter-vehicle gaps become smaller this methodology prohibits the system from making lane changes. Such a scenario can be seen in Figure (1-1). Where a human driver will try

to squeeze in and provoke a (yielding) reaction from surrounding vehicles, the ADS-operated vehicle, or in this thesis equivalently named *ego-vehicle*, will have to abide by its safety margins. These safety margins, designed in order to guarantee the vehicle's ability to avoid a collision by braking, inhibit a possible lane change.

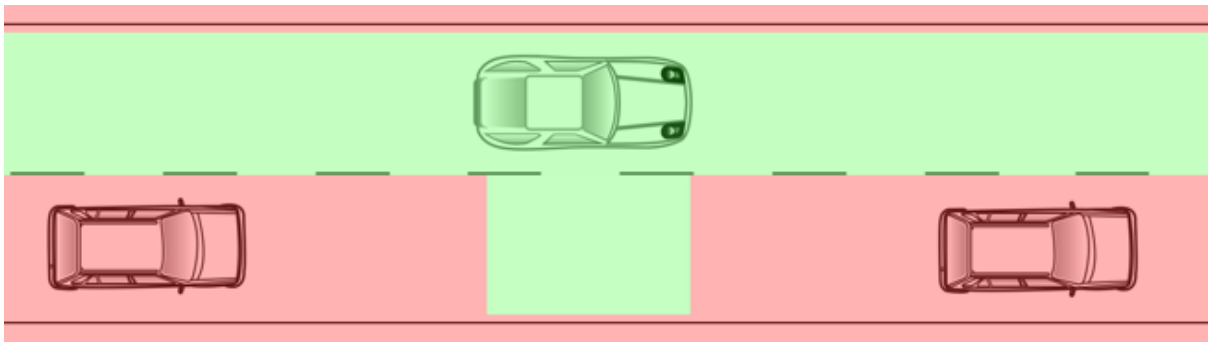

Figure 1-1: A possible merging scenario in dense traffic, where the red areas represent the ego-vehicles' safety margins and green is the allowed drivable area.

If however the ability of the system to abort the lane change, i.e. making a lateral (steering) maneuver is considered as well, the margins can be considerably reduced. This results in an increased availability of the lane change maneuver, as reported by Chandru et al[3]. In their solution the safety zones can be visualised as can be seen in Figure (1-2). From the figure it is evident that in a similar traffic-situation the ADS can now let the vehicle intrude in the target lane. This results in 'human-like' behaviour, making *active* lane changes by pushing into gaps, as opposed to Volvo's current solution of hanging on the lane edge with the indicator turned on, hoping for a polite reaction of fellow road-users.

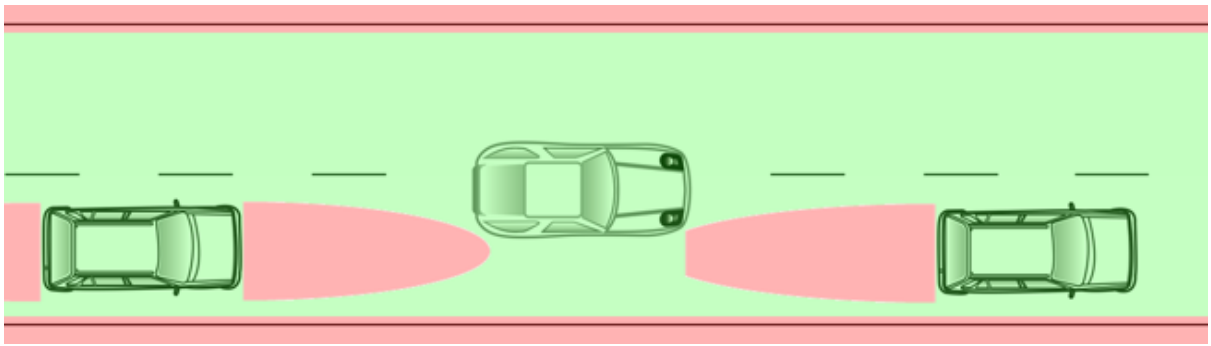

Figure 1-2: A possible merging scenario in dense traffic, where the red areas represent an artist impression of the ego-vehicles' safety margins and green is the allowed drivable area.

The theory behind this safety zone representation is that as long as the ADS-operated vehicle does not intrude in those areas, the ADS will have a collision avoidance maneuver available in the event of predefined set of incidents on which the design is based. These zones however do not have a fixed size, nor are they purely speed-based as the conventional approach and Chandru's implementation[3]. Intuitively the reader can already imagine an evasion-maneuver by the vehicle will also be influenced by its relative angle toward the object it is trying to avoid.

The key is therefore to develop a path planning algorithm which takes the lateral evasion capability into account but at the same time guarantees the validity of the safety zone for every possible combination of surrounding- and ego-vehicle states, and adheres to its boundaries. Further requirements on the algorithm are that it should be real-time feasible and be able to take vehicles into account in both target and host lane.

1-2 Thesis Contribution

The author of this thesis has collaborated with Volvo Cars and it's subsidiary Zenuity to continue research based on the work done earlier by Chandru et al[3] and to develop a lane change path planning algorithm based on the philosophy of using the ADS-operated vehicle's evasion capabilities to define the margins taken into account with respect to surrounding traffic.

In this thesis, these requirements are (mathematically) formalized and a methodology is developed such that they can be applied in a Model Predictive Control (MPC) strategy. A computationally expedient system model that adequately represents vehicle heading is chosen, and the scheme is subsequentially implemented using a state-of-the-art nonlinear optimisation solver not used earlier for such an application.

The author's specific contribution lies in the development of a formulation which includes the vehicle's heading, thus making the methodology safe, and developing a 3-step framework to implement this formulation, while allowing it's use on multiple vehicles spread over different lanes, and as well being able to plan an overtaking maneuver.

The developed algorithm is produced in matlab-code in combination with a C-code generated solver, and is designed to allow future in-vehicle validation.

1-3 Thesis Outline

The next chapter will give an introduction to path planning with safety requirements, introducing different methods and detailing why MPC is chosen in this project. After that Chapter 3 will introduce the modelling used for the vehicle, road, objects and traffic to accurately represent them in the Model Predictive Control framework. Chapter 4 will then introduce the concept of the safety zone and detail the equations that are developed to represent it. Next, Chapter 5 describes the 3-step methodology devised to implement the safety zone equations and at the same time be able to take surrounding traffic into account. The methods and tools used to achieve a real-time implementation will then be explained in Chapter 6. The results are presented and analyzed in Chapter 7 after which a retrospective is given in Chapter 8 including a conclusion, a discussion of the limitations of this work and suggestions for future work.

Chapter 2

Path Planning

Path planning is a broad term, but in an automotive setting it usually involves finding a way from point A to B. In this setting it can be divided into two further classes:

1. Global path planning
2. Local path planning or trajectory generation

Global path planning is a very high level process and is concerned with determining which roads, highways, tunnels, boats or bridges to take to get the shortest or quickest route from the travel starting point to the final destination. Nowadays this task is very often dedicated to a satellite navigation system, which uses increasing amounts of live information such as accident notifications and traffic flow measurements to determine which route the driver or car should take.

Local path planning is concerned with following the globally planned path on a local scale, meaning from the vehicles exact location on the road up to about 100-200[m] in front of it, depending on velocity. This means navigating around a bend, changing lanes on the highway or slowing down for traffic. In a manually-operated vehicle the planning of such maneuvers is all done in the drivers head, as he decides which lane to drive in and how to operate the steering wheel in order to achieve it. In an ADS-operated vehicle this driving task consists of three parts:

1. Collecting information from sensors and fusing it with available (online) data such as road maps into a workspace
2. Planning a path and calculating corresponding control inputs
3. Execute control input through actuators

The main focus of this thesis is the design of the control algorithm to execute step 2. For the purpose of this thesis, the definition of ADS path planning is formulated as follows:

> "Generating a set of consecutive longitudinal and lateral coordinates over a planning horizon, including either or both other vehicle states such as speeds, headings and accelerations that can be tracked by a lower level controller, or a set of control inputs for the vehicle actuators, that when executed form a path which is feasible, meeting requirements on comfort, safety, collision avoidance." [6]

From this definition a number of requirements on a path planner and/or the planned path can be derived:

- The path must be followable, so it must be planned with the vehicle dynamics kept in mind
- The path must be comfortable: passengers should under normal operation experience a pleasant ride
- It should be collision-free: the planned path should not collide with any obstacles or other road users
- It should be safe and robust to prediction error: if a current path is found, through new sensor information, to suddenly cause a collision, the vehicle should be able to avoid it.

All of these statements need to be specified to be turned into more formal requirements on the path or the path planner. Which vehicle dynamics are to be taken into account and how is the subject of Chapter 3. The definition of 'comfortable ride' can be turned into a set of comfort limits on vehicle acceleration and jerk, and the values of these are a widely debated topic. For this thesis the values found by Eriksson et al[7], at $a_y = 2[\mathrm{m/s^2}]$ and $j_y = 0.9[\mathrm{m/s^3}]$ will be used as maximum measures for comfort. This leaves the collision avoidance and the safety statement to be discussed in the following section.

2-1 Safe Path Planning

Planning a collision-free path means planning a path that it does not collide with any fixed road obstacles or other vehicles, based on their movement predictions. There are numerous ways to achieve this, but the most important ones fall into one of the following three classes[8]:

1. Planning a path using a policy-based algorithm, such as machine learned neural-network. In order to guarantee collision avoidance the control algorithm has to be simulated for a large number of situations to provide statistical proof
2. Using sampling-based methods such as RRT to plan a large number of paths and using a collision avoidance checking algorithm to choose the path that does not collide with anything
3. Providing collision avoidance as constraint for an optimisation based path planner such that any solution coming from the algorithm is collision-free.

Using statistical analyses it is very hard to provide a 100% guarantee on collision avoidance, and to get close an extremely large amount of simulations is necessary[9] which makes it an unfavourable candidate. It is therefore that preference goes out to a deterministic proof of collision avoidance, for example by post-checking that a path is collision-free.

Doing so when planning a path with regards to fixed obstacles such as guard rails or road works is relatively straight-forward, as when you have a path which can dynamically be followed by the vehicle, that does not intersect with the location of the obstacle, it will not collide with it, as a fixed obstacle does not move.

When planning a path in between other vehicles on the road however, this guarantee is not so easily made. Planning a collision-free path then involves predicting the trajectories of the

surrounding vehicles which, when wrong, can lead to collisions. This means that even when the predictions are really accurate, unless they are guaranteed to be 100% correct, the path still needs to be robust towards prediction error in order to place guarantees on safety.

For obvious reasons, it is important that ADS path planning is safe. How safe exactly is an ongoing debate[5], and to define what is safe and what is not can be a tedious exercise. It is however possible to say that the path planning solution should be able to handle a certain set of unpredictable events or types of possible accidents.

The guarantees that can be made with regards to safety go hand in hand with the unpredictable events that are taken into account when designing the path planner. The set of unpredictable events basically form the robustness requirement: they define which events or situations (that result in unpredicted changes in the constraints) the controller should be able to cope with.

Based on the situation of driving on a highway or closed causeway with separated lanes, there are two main events that will be taken into account in this thesis. The first one is a braking maneuver from a leading vehicle in either the host or target lane, with the worst-case being an instant stop, and the second one is a cut-off maneuver from a trailing vehicle in the target lane, with a worst-case maximum acceleration of 10 m/s^2 at high friction conditions.

This set of unpredicted events that should be accounted for, the control action available to the controller and the system's driving behaviour all stand in direct relation to each other (Figure 2-1). The goal of this thesis is to enable the path planner to initiate tighter mergers and make more active lane changes. As the **events** are defined, in order to influence this driving **behaviour**, the available mitigation **actions** of the controller need to be extended. Until now control actions considered by Volvo for mitigation in a lane change scenario were limited to braking, resulting in the conservative behaviour discussed in Section 1-1. Brännstrom et al[10] have shown however that when a lateral margin of 1[m] is available, steering provides a quicker collision avoidance maneuver than braking at speeds higher than 17[m/s], going down to 14[m/s] when 3[m] lateral margin is available. In order to enable the new merging behaviour at highway speeds of 20[m/s], in this thesis the available control actions will be extended by steering, adding the ability to perform an evasive maneuver.

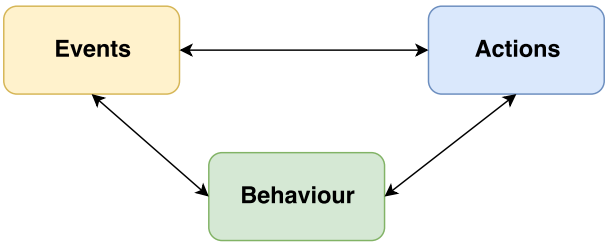

Figure 2-1: Relationships between the controller design parameters.

Now that the events and actions are defined, they can be used to design the path-planning algorithm. In lane-change path planning, the main maneuver considered in this thesis, guaranteeing safety comes down to the availability of a back-up maneuver at all times during the lane change, such that it can be chosen if the original path is going to result in a collision because of prediction error.

For a sampling based method to have a back-up maneuver available at every point on the predicted path would mean planning as many back-up paths as there are points on the horizon (see Figure (2-2)), and having each of them checked for collisions with the leading vehicle. As post-checking for collision avoidance on RRT paths is already computationally demanding[8], collision avoidance checking for all possible back-up paths would be a very time consuming task, prohibiting the real-time implementation of such an algorithm. If however a mathematical

constraint formulation can be found to guarantee the availability of the backup maneuver, this constraint could be implemented in an optimisation-based path planning algorithm and enforced at every point along the prediction horizon.

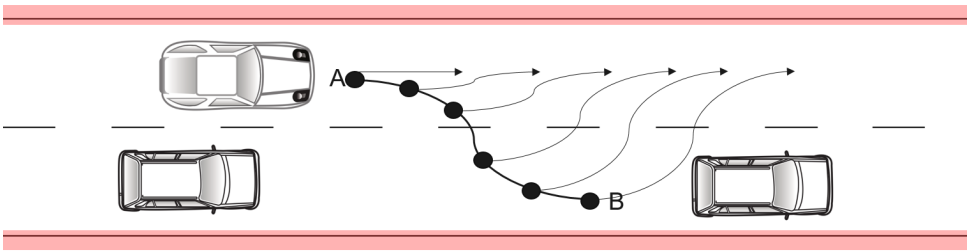

Figure 2-2: Driving situation showing what it would look like to plan a path into a gap, and plan an evasion maneuver for each step on the prediction horizon.

Fortunately, such a mathematical constraint formulation was developed by Chandru et al[3] and the extension guaranteeing safety is one of the main contributions of this thesis. It is part of what will be called 'the safety zone' and its design will be treated in Chapter 4 of this thesis.

Together with this constraint formulation, an optimisation-based path planner can be used to generate lane change trajectories with guarantees on safety. In order to get to this implementation, the next section will deal with the design of such a path planner, specifically one using Model Predictive Control.

2-2 Receding Horizon Control

In optimisation-based path planning a path is the result of a constrained finite time optimal control problem bringing the vehicle to a certain final state, with a cost function taking into account factors such as comfort and safety.

In its general form, an optimal control problem is described by equations (2-1) to (2-7).

$$\min_{x(t),u(t)} J(x(t),u(t)) \tag{2-1}$$

$$J(x,u) = \int_0^{T_f} (x(t)-x_{ref})^2_Q + (u(t)-u_{ref})^2_R \tag{2-2}$$

$$s.t. \tag{2-3}$$

$$\dot{x} = f(x(t),u(t)) \tag{2-4}$$

$$x(t) \in \mathcal{X} \tag{2-5}$$

$$u(t) \in \mathcal{U} \tag{2-6}$$

$$g(x,u) \leq 0 \tag{2-7}$$

The solution to the OCP is the result of minimizing (2-1) the cost function $J(x,u)$ (2-2), where Q and R are the weighting matrices that determine how much each of the state and control errors respectively, are penalized. These weightings are therefore also the tuning parameters that determine the behaviour of the controller. This minimization is subject to vehicle dynamics (2-4) which will be discussed in Chapter 3, the constrained set of allowable states $\mathcal{X}$(2-5) and $\mathcal{U}$(2-6) which will be defined by state boundaries such as a speed limit, and actuator limitations, and the inequality constraints (2-7) which will contain all of the collision avoidance formulations.

The solution to this optimisation will then be a series of state evolutions x and corresponding control inputs u which form the optimal path towards the given objective.

Minimizing the cost function can be done offline, as used to be the practice in planning spacecraft trajectories. However in order to be robust to prediction errors, and to be able to account for fluctuating constraint values as a result of the constantly changing traffic environment, it is necessary to continuously reiterate this optimisation online. After each iteration the first control input is implemented (or the first set of states is passed to lower-level controller) after which the optimisation is repeated and the rest of the old solution is discarded in favour of the new one. Figure 2-3 shows a schematic of such a strategy, which is called Reciding Horizon Control (RHC) or Model Predictive Control (MPC).

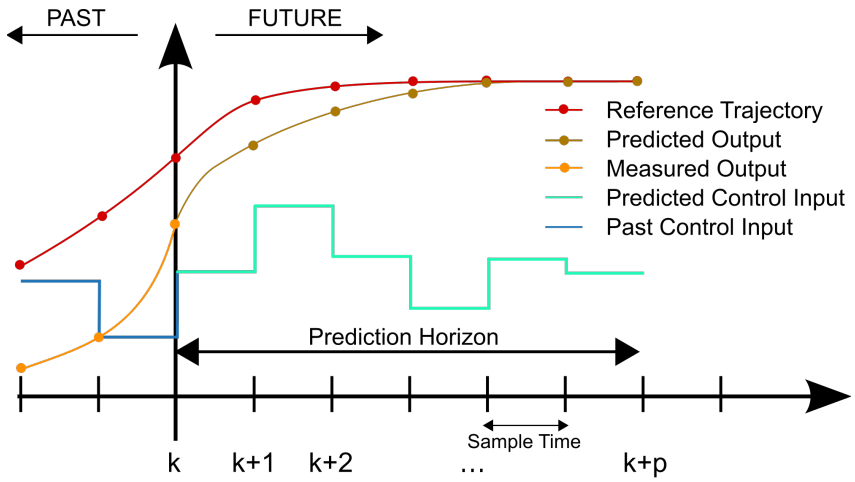

Figure 2-3: Receding Horizon Control schematic. Source [1].

The exact set up of the Optimal Control Problem (OCP) will be discussed in Chapter 5, after the vehicle dynamics, road frame and corresponding state constraints have been defined in Chapter 3 and the collision avoidance constraints have been formulated in Chapter 4.

Chapter 3

Models

In this chapter, the modelling of the vehicle dynamics will be considered, but also the modelling of the surroundings and traffic to be able to use them in a time-dependent Model Predictive Control (MPC) framework. Furthermore the modelling of the evasion maneuver will be considered seperately from the vehicle dynamics.

3-1 Vehicle Model

The general rule of thumb is to define the dynamics of the system to be controlled as accurately as possible. In model predictive control, due to the dynamics appearing in every optimisation step, a trade-off has to be made with regards to model accuracy and computation time.

Based on earlier research [11], a simplified single-track model is chosen to represent the vehicle dynamics, as a trade-off between the point-mass model[12] which does not include any of the heading dynamics crucial to this research, and the 4-wheel dynamic model which includes load transfer and other higher order elements[13] increasing computational complexity.

In a straight road scenario the simplified single track model is described by equations (3-1) to (3-5), where a_x and δ_{rate} are the inputs.

$$\dot{x} = vcos(\psi) \tag{3-1}$$

$$\dot{y} = vsin(\psi) \tag{3-2}$$

$$\dot{\psi} = \frac{v}{l(1 + (\frac{v}{v_{ch}}^2))} \cdot \delta \tag{3-3}$$

$$\dot{v} = a_x \tag{3-4}$$

$$\dot{\delta} = \delta_{rate} \tag{3-5}$$

In this model the vehicle parameters have been collected in the characteristic velocity v_{ch} which is described by equation (3-6).

$$v_{ch} = \sqrt{\frac{l^2 c_f c_r}{m(c_r l_r - c_f l_f)}} \tag{3-6}$$

In these equations l represents the vehicle axle length, with l_f and l_r the distances from the center of gravity to the front and rear axle respectively. The tyre dynamics are approximated

in this defintion using a front c_f and rear c_r cornering stiffness. This approximation is valid as long as slip angles remain small[14], which is enough to accommodate the nominal driving scenario's in this thesis.

The framework however does extend to more extreme situations, which is why evasion maneuver planning is also included into the results (section 7-3). However to implement the evasion scenarios it is advisable extend the control scheme by using lower level controllers to track the state and control trajectories. The nonlinear tyre dynamics can then be taken into account in the lower level control, but that is not part of this research.

To make sure that the planned paths however stay within the physical limits of the tyres, the longitudinal and lateral acceleration are bounded by the tyre friction circle; leading to the constraint in equation (3-7).

$$(a_x)^2 + (v\dot{\psi})^2 \leq \mu^2 g^2 \tag{3-7}$$

Further advantages of using this model include the non-singularity at $v = 0$ allowing full stop braking, and the dynamics are non-stiff which allows a relatively large step size benefiting overall computation time[11].

3-2 Road Frame

The single-track model can be adapted to allow the implementation of a curved-road framework by introduction of the road frame variables described by equations (3-8) to (3-10).

$$\dot{y}_r = vsin(\psi - \psi_r) \tag{3-8}$$

$$\dot{\psi}_r = \frac{vcos(\psi - \psi_r)}{1 - y_r\kappa_r(s_r)}\kappa_r(s_r) \tag{3-9}$$

$$\dot{s}_r = \frac{vcos(\psi - \psi_r)}{1 - y_r\kappa_r(s_r)} \tag{3-10}$$

Here, ψ_r describes the road angle in a global frame, and s_r is the 'arc length', the travelled distance in the road frame. y_r can then be described as the lateral error towards the road frame. The curvature of the road $\kappa(s)$ is equal to the reciprocal of the curve radius, $\frac{1}{\rho(s)}$. A diagram clarifying these relationships can be seen in figure 3-1.

It can clearly be seen that in a straight road scenario, where $\kappa(s) = 0$, and $\psi_r = 0$; the following holds:

$$\dot{y}_r = \dot{y} \tag{3-11}$$

$$\dot{\psi}_r = \dot{\psi} \tag{3-12}$$

$$\dot{s}_r = \dot{x} \tag{3-13}$$

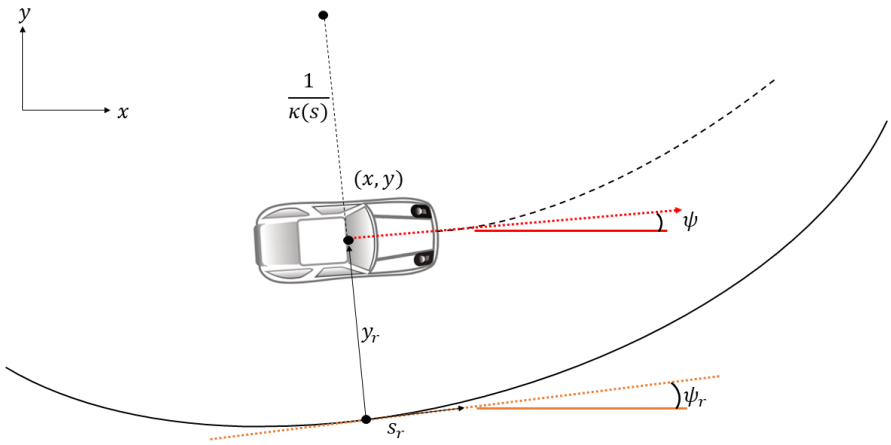

Figure 3-1: Curved road single-track model.

To simplify further formulations this thesis will focus on a straight road scenario, but the statements and formulations can easily be extended to the curved road framework by replacing the variables x, y and ψ with their curved road frame equivalents unless otherwise stated in later paragraphs.

3-3 Spatial Constraints

The next step is to define road edges and obstacles in such a way that they can be implemented in the Optimal Control Problem. When looking at the example in figure 3-2 the obvious way to present the tree on the road, which at the current speed lies 3 seconds ahead of the ego-vehicle, is as a change in the lateral constraints. The lower constraint on position y would then change from $y_{min} = 0$[m] to $y_{min} = 4$[m], on the prediction horizon at t = 3[s], forcing the ADS to let the vehicle make a lane change. However when the system speeds up the vehicle from its current speed, the tree will not be 3 seconds ahead but less, resulting in a possible collision because the ego-vehicle has not completed its lane change yet.

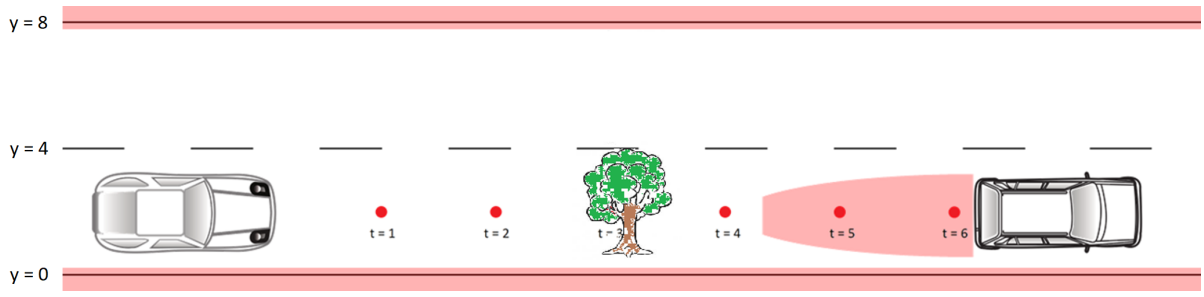

Figure 3-2: Road constraints on a time-based prediction horizon.

In order to tackle this problem the constraints with a fixed location such as obstacles on the road, lane edges, (road curvature in the curved road frame) and speed limits will be defined as functions of the longitudinal position x (or arc length s_r). This way they will always have a correct position on the prediction horizon irrespective of the planned path.

$$\overline{y} = f(x), \underline{y} = f(x), \overline{v} = f(x) \tag{3-14}$$

Some of these functions however involve step functions. Since the nonlinear solvers require continous functions (refer to Chapter 5 for further explanation) a polynomial approximation has to be made, resulting in the constraint formulation in equations (3-15) to (3-17) as seen in [15].

$$\overline{y}(x) = k_0 + k_1 x(t) + k_2 x(t)^2 + k_3 x(t)^3 + ... \tag{3-15}$$
$$\underline{y}(x) = k_0 + k_1 x(t) + k_2 x(t)^2 + k_3 x(t)^3 + ... \tag{3-16}$$
$$\overline{v}(x) = k_0 + k_1 x(t) + k_2 x(t)^2 + k_3 x(t)^3 + ... \tag{3-17}$$

Making these polynomial approximations should be done based on the sensor and road-map information, and is not part of this thesis. It is relevant to describe the approach however, to reinforce the proposition of Model Predictive Control as a path planning methodology. In this thesis, these constraint functions will be precomputed and supplied to the control algorithm by the simulated perception module, which will later be discussed in Chapter 7.

3-4 Evasion Maneuver

In order to reduce the computation complexity of the collision avoidance constraint, the evasion maneuver is chosen to be modeled using the point-mass model:

$$\dot{x} = v_x \tag{3-18}$$
$$\dot{v} = a_x \tag{3-19}$$
$$\dot{y} = v_y \tag{3-20}$$
$$\dot{v_y} = a_y \tag{3-21}$$

Further detail on how the safety zone is designed can be found in Chapter 4 and Chapter 5, this section will focus on the validation of the point-mass model for the evasion maneuver, as seen in Figure 3-3.

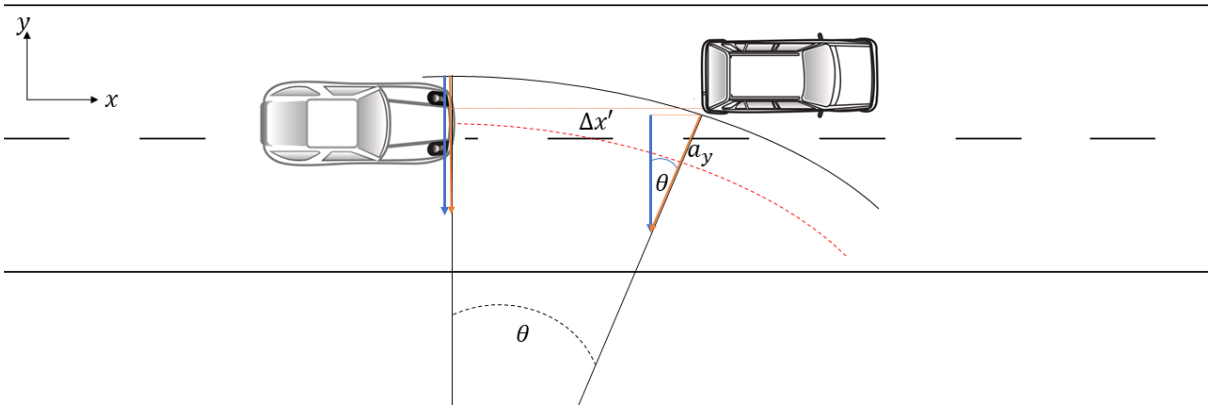

Figure 3-3: Evasion maneuver modeled as a steady-state cornering circle.

For the quickest evasion maneuver a constant maximum lateral acceleration of a_y in the vehicle reference frame is chosen. 8 [m/s^2] longitudinal acceleration should be available to make hard braking maneuvers, as the assumption on the safety zone only says the area right next to the ego-vehicle should be empty, so there could still be vehicles further forward in the right lane. Assuming again a high friction situation ($\mu \approx 1$), then using (3-7) the available lateral acceleration is:

$$a_{y,max} = \sqrt{(\mu g)^2 - a_x^2} \approx 5.7$$

When a vehicle is performing a steady-state cornering maneuver, the path of the vehicle can be described by a circle (3-22). The maximum lateral acceleration is in the vehicle reference frame, so after travelling a certain distance θR along the circle, the global (point-mass) reference frame lateral acceleration will now be $a_{y,global}$ (3-23) instead of a_y.

$$R = \frac{v^2}{a_y} \tag{3-22}$$

$$a_{y,global} = cos(\theta) \cdot a_y \tag{3-23}$$

$$\theta = \tan^{-1} \frac{\Delta x'}{R} = tan^{-1}(\frac{\Delta x'}{v} \cdot \frac{a_y}{v}) \tag{3-24}$$

The angle θ travelled is described by the distance between the two vehicles $\Delta x'$ and the radius R through equation (3-24). The safety zone is mostly relevant when driving at (sub)-1[s] gaps ($\frac{\Delta x'}{v} \leq 1$), so with a safety zone designed for maximum 5.7[m/s^2] at the minimum relevent speeds of 15 [m/s], the maximum deviation between a_y and $a_{y,global}$ is:

$$cos(\theta) = cos(tan^{-1}(1 \cdot \frac{5.7}{15})) \approx 0.93$$

In conclusion, when a $\sim 7\%$ margin is taken into account when communicating the maximum available lateral acceleration to the path planner, the point-mass model maneuver is accurate enough to base the design of the safety zone on. Therefore a maximum lateral acceleration of 5[m/s^2] will be considered in this work.

Chapter 4

Safety Zone

As discussed in Chapter 2, the availability of the lane change maneuver can be increased (drastically) if an evasion or abort-maneuver is available during the lane change as compared to the a braking-only maneuver. Instead of planning this evasion maneuver explicitly for the entire planned path, the model predictive control methodology presented in Section 2-2 allows the implementation of a constraint formulation to ensure the availability along the complete prediction horizon, if such a formulation exists.

To come to this collision avoidance constraint, two formulations must be looked at; namely the Time-To-Collision (TTC) and the Avoidance-Maneuver-Time (AMT). The Time-To-Collision is defined as the time it would take, based on the current ego-vehicle speed, to collide with a certain target vehicle or object under the worst-case incident assumption (e.g. harsh braking or a sudden stop). The Avoidance-Maneuver-Time is the minimum time needed for the ego-vehicle to avoid a collision in such a scenario, which can be based on either a braking or a steering maneuver.

As long as the Time-To-Collision then remains larger than the Avoidance-Maneuver-Time this means that the worst-case assumed incident can be avoided should it occur. By formulating the TTC and AMT as functions of the vehicle's states this inequality (4-1) can be applied as a constraint on the optimisation. This then results in the desired guarantee that at any point, along any generated path the ego-vehicle maintains the ability to avoid the assumed incident.

$$TTC \geq AMT \tag{4-1}$$

The formulations of the TTC and AMT depend on the dynamic modelling of the incident and abort situation and will be introduced in Sections 4-2 and 4-3 respectively. Before moving onto the modeling of these situations, the naming convention and the assumptions taken into account will be discussed in Section 4-1.

4-1 Assumptions and Naming Conventions

In order to explain the different road situations and to refer to the vehicles correctly, the followning naming conventions are made:

- The ego-vehicle is the vehicle to be controlled, and shall in figures always be depicted by the depicted model indicated with 'ego' in Figure (4-1).

- The surrounding vehicles, or surrounding traffic is the combination of vehicles numbered 1, 2 and 3 in Figure (4-1). A surrounding vehicle (non-ego-vehicle) will always be depicted with the car model used here.
- The host-lane is the lane the ego-vehicle is driving in.
- The target-lane is the lane indicated by the lateral reference.
- The direction of driving is to the right in all figures, and the right lane is thus equivalent to the lower lane, and the left lane equivalent to the upper lane.
- A leading or lead-vehicle is a vehicle who's Centre of Mass is in front of the ego-vehicle's. In Figure (4-1) both vehicles 2 and 3 are lead-vehicles.
- A trailing vehicle is a vehicle who's Centre of Mass is behind the ego-vehicle, such as vehicle 1 in Figure (4-1).
- The vehicle numbering as in Figure (4-1) will be consistent throughout the thesis. This means the most forward vehicle in the left lane will always be vehicle 2, followed by vehicle 1. The vehicle in the right lane will be referred to as vehicle 3.

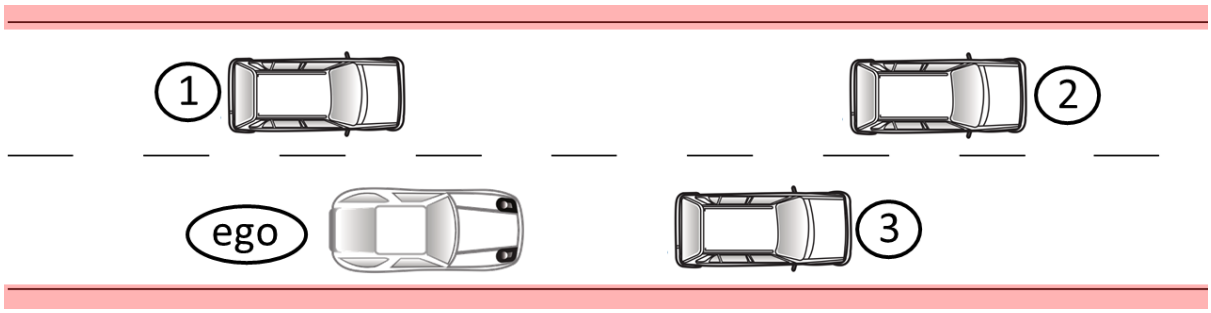

Figure 4-1: The numbering convention for the surrounding vehicles.

With the naming conventions clear, the assumptions on the surrounding vehicles and worst-case scenarios can be made. These assumptions will have a clear influence on the path planning solution and how it is designed.

1. The surrounding vehicles will always keep lane, and only longitudinal actions will be accounted for, thus acceleration or braking by trailing or leading vehicles.
2. The worst case assumption on the longitudinal movement is a sudden stop by a leading vehicle, and a maximum acceleration of $8[\mathrm{m/s^2}]$ by a trailing vehicle.
3. The worst case scenario will only affect 1 of the surrounding vehicles directly at any given time.
4. A steering-only maneuver will be used to base the AMT on.
5. A constant acceleration model will be used to approximate the dynamics of the evasion maneuver to facilitate explicit modeling. The maximum lateral acceleration $a_{y,max} = 5[\mathrm{m/s^2}]$.
6. The area immediately next to the ego-vehicle is presumed to have an empty (evasion) space for at least one vehicle length. If this space is predicted to disappear, the lane change should be aborted.

4-2 Time-To-Collision

As said, the Time-To-Collision corresponding to a target-vehicle driving in front of the ego-vehicle will be based on the time it takes for the ego-vehicle to collide with the target-vehicle in case it comes to a sudden stop and the ego-vehicle does not react in any way. A possible vehicle positioning during a lane change can be seen in Figure (4-2).

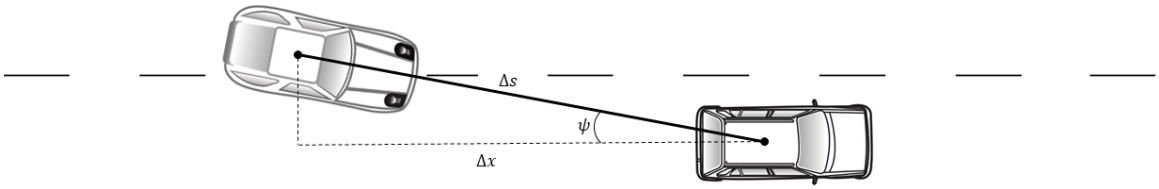

Figure 4-2: Vehicle configuration to explain TTC formulation for a leading vehicle.

The expression of the Time-To-Collision to the target vehicle then follows in equation (4-3).

$$TTC_{lead} = \frac{\Delta s}{v_{ego}} = \frac{\frac{\Delta x}{cos(\psi)}}{v_{ego}} = \frac{\Delta x}{v_{x,ego}} \tag{4-2}$$

In this equation Δs is the absolute distance between the ego-vehicle and target-vehicle, and Δx the distance in the longitudinal frame (or along the road, in case of the curved road frame). To account for the vehicle lengths they have to be substracted from the relative distance between the two vehicles:

$$TTC_{lead} = \frac{\Delta x - \frac{1}{2}L_{ego} - \frac{1}{2}L_{object}}{v_{x,ego}} \tag{4-3}$$

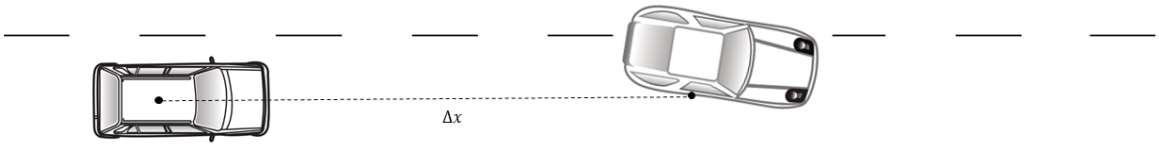

Figure 4-3: Vehicle configuration to explain TTC formulation for a trailing vehicle.

The **TTC** for a vehicle in the rear (TTC_{trail}) is based on the worst-case expected acceleration a trailing will vehicle will make to cut the merging ego-vehicle off. A definition for the TTC can be derived by setting the final position of the ego- and leading vehicle equal:

$$x_{ego,final} = x_{trail,final} \tag{4-4}$$

$$x_{0,ego} + v_{ego}\Delta t = \frac{1}{2}a_{trail}\Delta t^2 + v_{trail}\Delta t + x_{0,trail} \tag{4-5}$$

$$TTC_{trail} = \Delta t = \frac{v_{ego} - v_{trail}}{a_{trail}} + \frac{1}{a_{trail}}\sqrt{2(x_{0,ego} - x_{0,trial})a_{trail} + (v_{trail} - v_{ego})^2} \tag{4-6}$$

Again taking into account the vehicle's length, this leads to:

$$TTC_{trail} = \frac{v_{ego} - v_{trail}}{a_{trail}} + \frac{1}{a_{trail}} \sqrt{2(x_{0,ego} - x_{0,trial} - \frac{1}{2}L_{ego} - \frac{1}{2}L_{object})a_{trail} + (v_{trail} - v_{ego})^2} \tag{4-7}$$

The next step is to calculate the Avoidance-Maneuver-Time.

4-3 Avoidance-Maneuver-Time

The avoidance maneuver time is a description of the time it will take to avoid an accident by making a lateral maneuver, for example moving back into the original lane during a lane change.

For this particular maneuver the vehicle is considered as a point-mass, as explained in Section 3-4 where a validation is given as well. Through making this assumption, the AMT can be seen as the time needed to travel a certain lateral distance, to a 'safe' lateral position.

In a point-mass frame the time needed to move a certain lateral distance (Δy) is defined by equation (4-8).

$$\Delta t = \sqrt{\frac{2 \cdot \Delta y}{a_{y,max}}} \tag{4-8}$$

To complete this definition Δy has to be defined. Although vehicle heading (ψ) does not play a role in the point-mass system, the initial heading of the vehicle at the start of the evasion maneuver can influence the lateral evasion distance. In Figure (4-4) a lane change situation is presented with no relative heading angle. In this situation the lateral evasion distance can be defined as in equation (4-9).

$$\Delta y = y_{ego} - y_{object} + \frac{1}{2}W_{ego} + \frac{1}{2}W_{object} \tag{4-9}$$

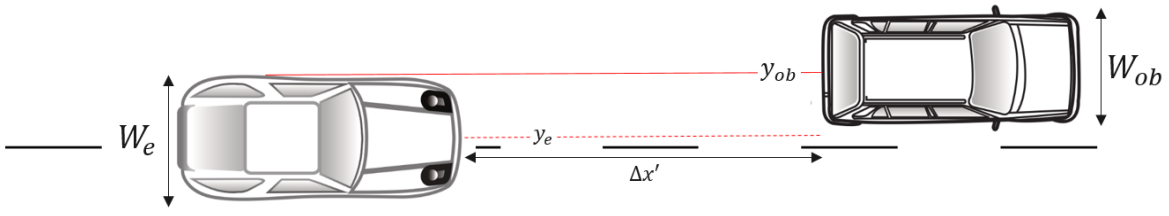

Figure 4-4: Vehicle configuration to clarify lateral evasion distance.

However, when the object to be evaded comes to a stop and the the ego-vehicle has a relative heading towards that vehicle, in the point-mass frame it will travel further into the target lane or gap as a result of its heading and longitudinal velocity. This 'extra' distance (Δy_ψ in Figure (4-5)) has to be added up to equation (4-9) to come to the right definition of the lateral evasion distance.

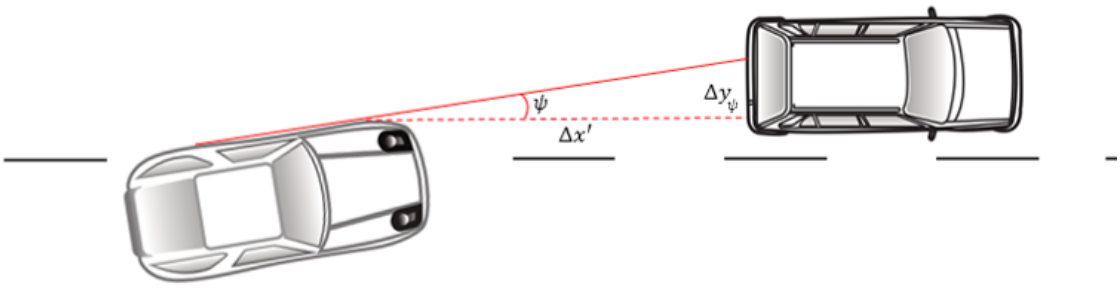

Figure 4-5: Vehicle configuration to clarify heading influence on lateral evasion distance.

Using the heading angle ψ, the definition of Δy_ψ can be presented in equation (4-10), after which the equation for the AMT is completed (4-11).

$$\Delta y_\psi = sin(\psi) \cdot \Delta x' \approx \psi \cdot \Delta x' \tag{4-10}$$

$$\Delta y = y_{ego} - y_{object} + \frac{1}{2}W_{ego} + \frac{1}{2}W_{object} + \psi \cdot \Delta x' \tag{4-11}$$

$$AMT = \sqrt{\frac{2 \cdot (y_{ego} - y_{object} + \frac{1}{2}W_{ego} + \frac{1}{2}W_{object} + \psi \cdot \Delta x')}{a_{y,max}}} \tag{4-12}$$

4-4 Curved Road Frame

As mentioned earlier most of the framework translates into a curved road framework by simply replacing variables x and y by their curved road equivalents. This also remains valid for the Time-To-Collision calculations. To translate the Avoidance-Maneuver-Time into the curved road framework on small addition has to be made, as heading angle of the road ψ_r might be different at the lead vehicle's position as can be seen in Figure (4-6).

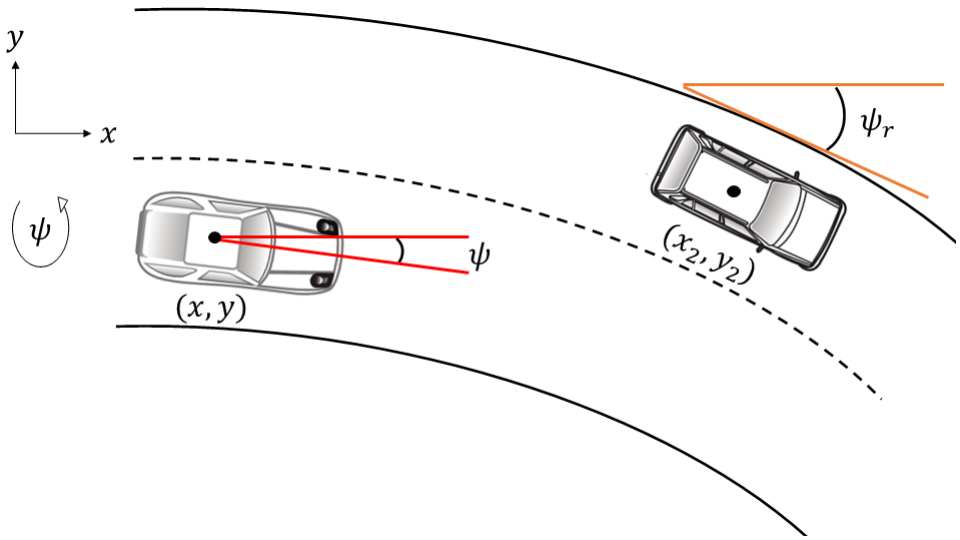

Figure 4-6: Safety zone headings in a curved road frame.

To take this into account, the heading ψ should simply be replaced by $\psi_{relative}$ (4-13). As mentioned before, this thesis will demonstrate it's control strategies in a straight road framework, but this simple addition is necessary when moving to a real-life application.

$$\psi_{relative} = \psi_r - \psi \tag{4-13}$$

4-5 The Safety Constraint Formulation

Finally collision avoidance would be ensured by enforcing the following constraint:

$$TTC \geq AMT \tag{4-14}$$

A more intuitive formulation, which at the same time eases implementation can be formulated as follows: if the distance that can be evaded in the time-to-collision is larger than that which needs to be evaded, the constraint is met.

$$\Delta s(TTC) \geq \Delta y \tag{4-15}$$

This formulation avoids the use of square roots, as can be seen in equation (4-16).

$$\frac{1}{2}a_{y,max} \cdot (TTC)^2 \geq y_{ego} - y_{object} + \frac{1}{2}W_{ego} + \frac{1}{2}W_{object} + \psi \cdot \Delta x' \tag{4-16}$$

In case of a vehicle in the front; the constraint on the variables x, y, v and ψ becomes:

$$\frac{1}{2}a_{y,max} \cdot (\frac{\Delta x'}{v_{obj} - v_{ego}})^2 \geq y_{ego} - y_{object} + \frac{1}{2}W_{ego} + \frac{1}{2}W_{obj} + \psi \cdot \Delta x' \tag{4-17}$$

$$\Delta x' = x_{obj} - x_{ego} - \frac{1}{2}L_{ego} - \frac{1}{2}L_{obj} \tag{4-18}$$

Now that the Time-To-Collision and Avoidance-Maneuver-Time have been defined and the constraint formulation to guarantee the availability of the evasion maneuver has been formulated, the implementation in the Model Predictive Control path planning framework can be defined in Chapter 5.

Chapter 5

Approach

The next step after having defined the safety zone constraint formulations in Chapter (4), is implementation using the Model Predictive Control framework. As explained in Chapter 3 a nonlinear model is used to represent the vehicle dynamics, in order to account for yaw behaviour but also to provide a coupling between the longitudinal and lateral movement of the vehicle: intuitively one can imagine that constraints on the longitudinal position of the vehicle (where it can be along the road) also depend on its lateral position (whether it moves in the right lane or the left); as you can drive in the same longitudinal position in the left lane while you pass another road user on the right.

This means the problem needs to be solved as nonlinear program. The previously defined functions for the safety zones for vehicles in the front and in the rear are naturally only valid when driving, respectively, behind or in front of a vehicle in question. In case the ego-vehicle is predicted to overtake such a vehicle, this means the constraint formulation will show a discontinuity when switching from the rear to the front safety zone.

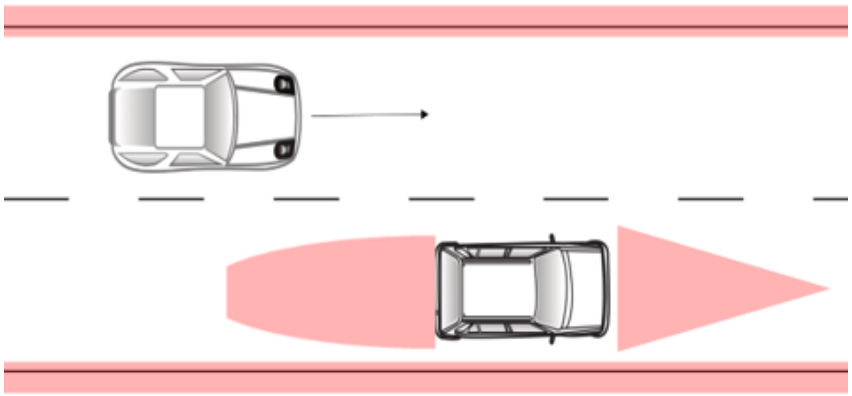

Figure 5-1: Artistic impression of the safety zones clarifying the switch from rear safety zone constraint to front safety zone constraint when overtaking a vehicle.

The methodology involved to solve the optimisation in the Model Predictive Control problem will be discussed in Chapter 6, but a key part involves computing gradients of among others the constraint functions, and as a result these need to be continuous, differentiable functions. In this chapter a tailored approach method will be discussed that was developed by the author to solve this problem.

5-1 3-step Approach

When the longitudinal planning (in the curved road frame longitudinal planning can be read as the arc length planning; the planning 'along' the path of the road) is determined, it is also clear when the ego-vehicle will be behind or in front of another vehicle, therefore determining which safety zone constraint should be active at which point on the horizon. By splitting up the path planning into a separate longitudinal and lateral planning, it is therefore possible to implement a constraint in the optimisation for a front- and a rearward safety zone for a certain vehicle, but to only activate the relevant one. This can be achieved by adapting the lower or upper bound to the safety zone inequality constraints online, based on the prediction of the surrounding vehicle movement.

However in order to use a pure decoupled longitudinal and lateral planning, it is necessary to have a 'predicted free zone'[2]: an area spanning the host- and target-lane containing no vehicles. This is necessary as surrounding vehicles translate to a constraint on longitudinal position depending on the ego-vehicle lateral position; and a constraint on lateral position depending on the ego-vehicle longitudinal position.

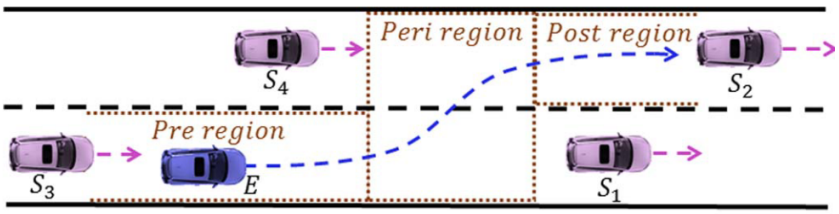

Figure 5-2: Schematic road view showing the 'predicted free zone' or 'peri region' necessary to plan a decoupled lane change maneuver. Image courtesy of Julia Nilsson[2]

In a dense traffic situation it is almost impossible to have such an area available. The problem can be solved however, by creating an initial path, providing an approximation of the ego-vehicle's position as function of time. If an estimate is available for a collision-free path, containing predicted values for vehicle longitudinal position, speed, lateral position and heading as a function of time $(x(t), v(t), y(t), \psi(t))$, then these can be used to generate a safety zone formulation depending only on $x(t)$ and $v(t)$ for the longitudinal planning, and one depending only on $y(t)$ and $\psi(t)$ for the lateral planning.

This results in a 3-step method: three optimisations are solved to find a final path which is collision-free and remains outside of the defined safety zones. The following sections will be used to detail the specific optimisation solved in each step.

5-2 Step 1: Combined Initial Planning

In the first step towards solving the trajectory planning a simplified path will be planned into the target gap. No safety zones or margins will be considered in this planning step, it serves only to generate first feasible coupled longitudinal and lateral path into the gap, which can then be used as a starting point for the separate longitudinal and lateral planning which will include the state-dependent safety formulations described earlier.

To generate a feasible and collision-free path the following constraints need to be taken into account:

$$0 \leq \overline{v}_x(x) - v_x \qquad \text{(speed limit)} \qquad (5\text{-}1)$$

$$0 \leq \overline{y}(x) - y \qquad \text{(upper lane boundary)} \qquad (5\text{-}2)$$

$$0 \leq y - \underline{y}(x) \qquad \text{(lower lane boundary)} \qquad (5\text{-}3)$$

$$\underline{a_x} \leq a_x \leq \overline{a}_x \qquad \text{(longitudinal acceleration)} \qquad (5\text{-}4)$$

$$\underline{\dot{\delta}} \leq \dot{\delta} \leq \overline{\dot{\delta}} \qquad \text{(steering rate limits)} \qquad (5\text{-}5)$$

$$(\overline{\mu} \cdot g)^2 \geq (a_y)^2 + (a_x)^2 \qquad \text{(friction limits)} \qquad (5\text{-}6)$$

Here constraint values for equation (5-1) to (5-3) and (5-6) are determined through sensor information from road signs (the speed limit) and the road situation (lane boundaries, road friction). Equations (5-4) to (5-5) are box constraints on the input to represent actuator limits.

Then in order to ensure the path does not collide with the (predicted) trajectories of the surrounding vehicles, a minimum distance keeping constraint is implemented on the Centre of Mass (CM) of the ego-vehicle. This constraint is based on a formulation by Weiskircher et al[15] and has an elliptical shape so that it is differentiable and can be processed by the nonlinear solver. The reasoning behind the sizing of this ellips can be seen in Figure (5-3), as this worst-case configuration must be the lower bound to the distance keeping constraint in order to keep the vehicles from colliding with each other.

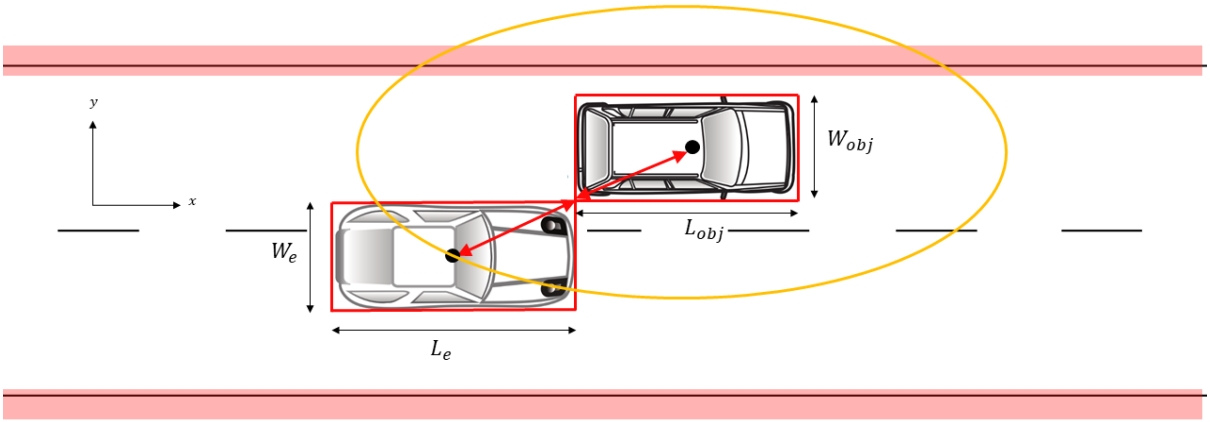

Figure 5-3: Largest distance between the two vehicles' CMs where they are still 'touching'. For simplification purposes the CM is chosen as the geometric centre.

The constraint is described in equation (5-7) for surrounding vehicles $i = 1...n$ with vehicle length L_i and vehicle width W_i. Although in this work a maximum of $n = 3$ surrounding vehicles was considered, the methodology extends to more vehicles if needed.

$$\left(\frac{x_{ego} - x_i}{\sqrt{2}(\frac{1}{2}L_{ego} + \frac{1}{2}L_i)}\right)^2 + \left(\frac{y_{ego} - y_i}{\sqrt{2}(\frac{1}{2}W_{ego} + \frac{1}{2}W_i)}\right)^2 \geq 1 \qquad (5\text{-}7)$$

Now that the inequality, state and input constraints have been defined, the OCP is formulated using equations (5-8) to (5-11), with the set of vehicles states $\mathcal{X}$ and controls $\mathcal{U}$ governed by model equations (3-1) to (3-5).

$$\mathcal{X} = [x, y, \psi, v, \delta] \tag{5-8}$$

$$\mathcal{Y} = [y, \psi, v] \tag{5-9}$$

$$\mathcal{U} = [a_x, \dot{\delta}] \tag{5-10}$$

$$\begin{aligned} OCP &= \min_{\mathcal{Y},\mathcal{U}} \int_{t=0}^{t_f} \left((\mathcal{Y} - \mathcal{Y}_{ref})^2 + \mathcal{U}^2\right) dt \\ &= \min \int_{t=0}^{t_f} \left(K_1(x - x_{ref})^2 + K_2(y - y_{ref})^2 + K_3(\psi - \psi_{ref})^2 + K_4(v - v_{ref})^2 + K_5 a_x^2 + K_6 \dot{\delta}^2\right) dt \end{aligned} \tag{5-11}$$

In the cost function x_{ref} is the longitudinal reference and is set at the position between the two vehicles that determine the gap. y_{ref} is the reference for the lateral position on the road, and its value either represents the center of the host lane, or, when a lane change is initiated, the center of the target lane. ψ_{ref} is usually kept at 0 or equal to the curvature of the road in the curved road framework. v_{ref} represents the reference speed and is dictated by either user setting or the road speed limit. K_1 to K_5 are the tuning parameters used to attain the desired controller behaviour. These can be changed online if necessary, and in this research two tuning sets are used: one for nominal driving, and one in case of an accident. When and if the weights are changed is decided by the higher level control architecture.

The model dynamics are time-dependent, while a number of constraints such as the speed limit, lane boundaries and (if included) road curvature are functions of the spatial position. This means they cannot be formulated as constraints on the time horizon, as their position on that horizon depends on the planning towards it. As, however, the position along the road x (or s_r in a curved road frame) is included as a variable, these constraints can be included as inequality constraints when they are approximated as polynomial functions:

$$\overline{v}(s) = c_0 + c_1 x(t) + c_2 x(t)^2 + c_3 x(t)^3 + ... \tag{5-12}$$

This overcomes the need to do a spatial transformation on the model dynamics. The polynomial approximations of road boundaries and speed limits as a function of longitudinal road position are presumed to be supplied by a separate precomputing module.

5-3 Step 2: Longitudinal Safety Planning

The result from step 1 will be a path from the ego-vehicle's current position into the target gap, guaranteeing a path is possible which doesn't collide with any surrounding vehicles, but only based on the provided prediction of the surrounding traffic. Based on the lateral planning of step 1, the ego-vehicle should hold a certain Time-To-Collision with regards to the surrounding vehicles to be able to deal with any deviations from this prediction. The goals of step 2 are thus two-fold:

1. Bring the ego-vehicle to the longitudinal position in the gap where the possible lateral intrusion is maximal
2. Maintain the correct Time-To-Collision towards surrounding vehicles based on the lateral planning of step 1

In order to achieve the first goal the point of maximum lateral intrusion, in other words the point where the ego-vehicle can go furthest into the gap without violating the safety constraints, has to be found. This point is indicated by the dotted line in Figure 5-4.

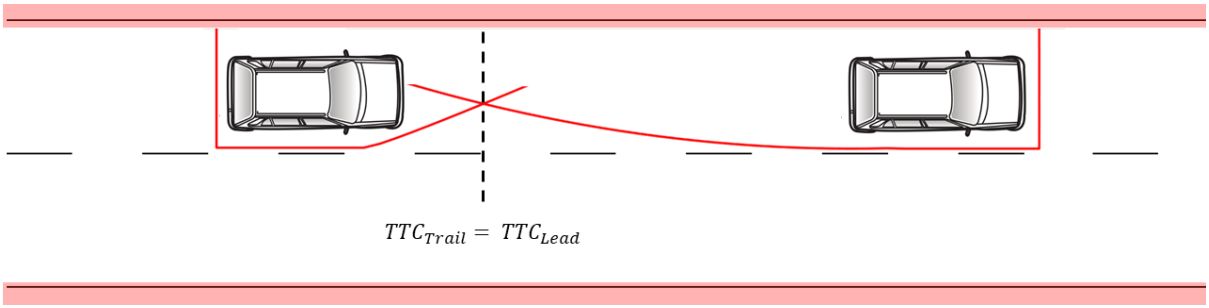

Figure 5-4: Safety zones around the surrounding vehicles for the predicted final position of the ego-vehicle in the gap.

In steady-state (with heading $\psi = 0$) the Avoidance-Maneuver-Time for a braking vehicle in the front is the same as for one one accelerating from the rear, provided their Time-To-Collision is equal. Therefore the point of maximum lateral intrusion occurs where the Time-To-Collision towards both vehicles is equal (equation (5-13)).

$$TTC_{lead} = TTC_{trail} \tag{5-13}$$

The cost function of the optimisation provides an excellent way of achieving this, by placing a cost on the difference between TTC_{lead} (4-3) and TTC_{trail} (4-7). Cost K_{11} will therefore determine the longitudinal attraction towards the target gap.

The second objective will be achieved by implementing the safety zone equation developed in chapter 4 (4-16). In order to implement this equation in the purely longitudinal optimisation the lateral part of the path planned in step 1 (heading ψ and lateral position y) will be used to define the constraint along the prediction horizon.

Based on the lateral planning of step 1 a longitudinal path without constraint violation might not be possible yet, therefore slack variables are included in the collision constraint formulation to create a soft constraint[16] that allows violation at the price of a high penalty. Any infeasible trajectory resulting from this violation should become feasible in step 3, if a feasible trajectory exists.

The longitudinal part of the dynamics is described by equations 5-14 and 5-15, however longitudinal jerk j_x is chosen as an input as opposed to longitudinal acceleration a_x. This way a cost can be placed to minimize jerk in order to generate comfortable trajectories.

$$\dot{x} = v_x \cos(\psi) \tag{5-14}$$
$$\dot{v}_x = a_x \tag{5-15}$$
$$\dot{a}_x = j_x \tag{5-16}$$

The following constraints will be placed on the states:

$$0 \leq \overline{v}_x(x) - v_x \qquad \text{(speed limit)} \tag{5-17}$$
$$\underline{a_x} \leq a_x \leq \overline{a}_x \qquad \text{(longitudinal acceleration)} \tag{5-18}$$
$$\underline{j_x} \leq j_x \leq \overline{j}_x \qquad \text{(longitudinal jerk)} \tag{5-19}$$

To maintain a hard collision avoidance constraint the elleptical constraint from step 1 (equation (5-7)) is copied however just as with the safety zone the lateral trajectory (indicated as $y(t)$) from step 1 is filled in to create a purely longitudinal constraint.

$$\left(\frac{x_{ego}-x_i}{\sqrt{2}(\frac{1}{2}L_{ego}+\frac{1}{2}L_i)}\right)^2 \geq 1-\left(\frac{\mathbf{y_{ego}(t)}-y_i}{\sqrt{2}(\frac{1}{2}W_{ego}+\frac{1}{2}W_i)}\right)^2 \tag{5-20}$$

The same goes for the safety zone constraint; the lateral variables are filled in based on step 1 data. The resulting rear-facing safety zone constraints (when driving behind another vehicle) are described by equation (5-21) for vehicles in the left lane, and equation (5-23) for vehicles in the right.

$$\frac{1}{2}a_{y,max}\cdot(\frac{\Delta x'}{v_i-v_{ego}})^2-\mathbf{y_{ego}(t)}+y_i-\frac{1}{2}W_{ego}-\frac{1}{2}W_i-\psi_{\mathbf{ego}}(\mathbf{t})\cdot\Delta x'\geq\zeta_i \tag{5-21}$$

$$\Delta x'=x_i-x_{ego}-\frac{1}{2}L_{ego}-\frac{1}{2}L_i \tag{5-22}$$

$$\frac{1}{2}a_{y,max}\cdot(\frac{\Delta x'}{v_j-v_{ego}})^2+\mathbf{y_{ego}(t)}-y_j+\frac{1}{2}W_{ego}+\frac{1}{2}W_j+\psi_{\mathbf{ego}}(\mathbf{t})\cdot\Delta x'\geq\zeta_j \tag{5-23}$$

$$\Delta x'=x_j-x_{ego}-\frac{1}{2}L_{ego}-\frac{1}{2}L_j \tag{5-24}$$

where the bold printed variables are know parameters from step 1, and $i=1..n$ are the surrounding vehicles in the left lane, while $j=1..m$ are the ones in the right lane. For the problem solved in this thesis, $n=2$ and $m=1$ vehicles are considered.

Following the same analogy, equations (5-25) and (5-26) describe the forward-facing safety zone (when driving in front of another vehicle) for vehicles in the left and right lane respectively.

$$\frac{1}{2}a_{y,max}\cdot(TTC_{rear,i})^2-\mathbf{y_{ego}(t)}+y_i-\frac{1}{2}W_{ego}-\frac{1}{2}W_i\geq\zeta_i \tag{5-25}$$

$$\frac{1}{2}a_{y,max}\cdot(TTC_{rear,j})^2+\mathbf{y_{ego}(t)}-y_j+\frac{1}{2}W_{ego}+\frac{1}{2}W_j\geq\zeta_j \tag{5-26}$$

where $TTC_{trail,i}$ and $TTC_{trail,j}$ are both described by equation (4-7) in Chapter 4.

Now that the inequality, state and input constraints have been defined, the OCP is formulated using equations (5-27) to (5-30), with the set of vehicles states $\mathcal{X}$ and controls $\mathcal{U}$ governed by model equations (5-14) to (5-16).

$$\mathcal{X}=[x,v_x,a_x] \tag{5-27}$$

$$\mathcal{Y}=[v_x,a_x] \tag{5-28}$$

$$\mathcal{U}=[j_x,\zeta_1,\zeta_2,\zeta_3] \tag{5-29}$$

$$\begin{aligned}
OCP &= \min_{\mathcal{Y},\mathcal{U}}\int_{t=0}^{t_f}\left((\mathcal{Y}-\mathcal{Y}_{ref})^2+\mathcal{U}^2\right)dt \\
&= \min\int_{t=0}^{t_f}\Big(K_7\cdot(v_x-v_{x,ref})^2+K_8\cdot a_x^2+K_9\cdot j_x^2 \\
&+ K_{10}\cdot\Big((\frac{x-x_i-\frac{1}{2}L_e-\frac{1}{2}L_i}{v_x})^2-(\frac{v_x-v_i}{a_i}+\frac{1}{a_i}\sqrt{a_i(x-x_i-\frac{1}{2}L_e-\frac{1}{2}L_i)^2+(v_x-v_i)^2)})^2\Big)^2 \\
&+ K_{11}\cdot\zeta_1^2+K_{12}\cdot\zeta_2^2+K_{13}\cdot\zeta_3^2\Big)dt
\end{aligned} \tag{5-30}$$

In this Optimal Control Problem-formulation three slack variables (ζ_i) have in included as inputs. These inputs will have very high related costs (K_{11} to K_{13}) and allow the formulation of the safety zone as 'soft constraints': constraints which can be violated, but at such a high cost that it will only happen if there is no other feasible solution. This will prevent the solver from aborting calculations due to infeasibility.

Furthermore weights K_7 to K_{10} are again tuned to achieve the desired controller behaviour, with two sets of parameters; one for nominal driving and one for a possible evasion maneuver, as discussed earlier in Section 5-2.

5-4 Step 3: Lateral Safety Planning

The third and last step consists of the lateral planning, fixing the longitudinal part of the dynamics by using the predicted state evolutions that resulted from step 2. Based on the ego-vehicles longitudinal planning the (predicted) TTC's for the surrounding vehicles can be determined, allowing the formulation of the safety zone constraint only depending on the lateral states y and ψ. With this constraint implemented, the lateral path can be planned such that it abides by the safety zones. The lateral model is described by equations (5-31) to (5-33).

$$\dot{y} = v_x \sin(\psi) \tag{5-31}$$

$$\dot{\psi} = \frac{v}{l(1 + (\frac{v}{v_{ch}}^2))} \cdot \delta \tag{5-32}$$

$$\ddot{\delta} = u_1 \tag{5-33}$$

In the Optimal Control Problem, the constraints in equations (5-34) to (5-38) will be implemented on the states.

$$0 \leq \overline{y}(x) - y \qquad \text{(upper lane boundary)} \tag{5-34}$$

$$0 \leq y - \underline{y}(x) \qquad \text{(lower lane boundary)} \tag{5-35}$$

$$-\frac{1}{2}\pi \leq \psi \leq \frac{1}{2}\pi \qquad \text{(heading)} \tag{5-36}$$

$$\underline{\delta} \leq \delta \leq \overline{\delta} \qquad \text{(steering angle)} \tag{5-37}$$

$$\underline{\dot{\delta}} \leq \dot{\delta} \leq \overline{\dot{\delta}} \qquad \text{(steering angle rate)} \tag{5-38}$$

As before, the distance keeping hard constraint is implemented to maintain a minimum distance to the surrounding vehicles, even when the safety zones are not activated (e.g. when the ego-vehicle is driving right next to another vehicle). Compared to the constraint in step 2, now the longitudinal part is known and the predicted state trajectory for $x(t)$ is filled in to create a constraint on just the lateral position.

$$\left(\frac{y_{ego} - y_i}{\sqrt{2}(\frac{1}{2}W_{ego} + \frac{1}{2}W_i)}\right)^2 \geq 1 - \left(\frac{\mathbf{x_{ego}(t)} - x_i}{\sqrt{2}(\frac{1}{2}L_{ego} + \frac{1}{2}L_i)}\right)^2 \tag{5-39}$$

This constraint is implemented for all vehicles ($i = 1:3$) irrespective of whether they're driving in the left lane or the right. Just as in step 2 a front-facing and rear-facing safety zone constraint is implemented for each vehicle. The rear-facing constraint for vehicles in the left lane ($i = 1, 2$) and the right ($j = 1$) are formulated in equation (5-40) and (5-42) respectively.

$$\frac{1}{2}a_{y,max} \cdot \left(\frac{\mathbf{\Delta x'(t)}}{v_i - \mathbf{v_{ego}(t)}} - 0.1 + \zeta_i \right)^2 - y_{ego} + y_i - \frac{1}{2}W_{ego} - \frac{1}{2}W_i - \psi_{ego} \cdot \mathbf{\Delta x'(t)} \geq 0 \quad (5\text{-}40)$$

$$\mathbf{\Delta x'(t)} = x_i - \mathbf{x_{ego}(t)} - \frac{1}{2}L_{ego} - \frac{1}{2}L_i \quad (5\text{-}41)$$

$$\frac{1}{2}a_{y,max} \cdot \left(\frac{\mathbf{\Delta x'}}{v_j - \mathbf{v_{ego}(t)}} - 0.1 + \zeta_j \right)^2 + y_{ego} - y_j + \frac{1}{2}W_{ego} + \frac{1}{2}W_j + \psi_{ego} \cdot \mathbf{\Delta x'(t)} \geq 0 \quad (5\text{-}42)$$

$$\mathbf{\Delta x'(t)} = x_j - \mathbf{x_{ego}(t)} - \frac{1}{2}L_{ego} - \frac{1}{2}L_j \quad (5\text{-}43)$$

In these equations the bold printed variables indicate the known parameters from step 2, and $i = 1..n$ are the surrounding vehicles in the left lane, while $j = 1..m$ are the ones in the right lane. The main differences with the safety zone in step 2 are the placement of the slack variable inside the Time-To-Collision (TTC) formulation, and the addition of a 0.1[s] margin onto that same TTC. This margin (see Frigure 5-5) is based on the sampling time ($T_s = 0.1[s]$) and is added to prevent the vehicle from entering the safety zone within the first sampling time after the front vehicle has stopped, as in the worst-case scenario the sensor information will be updated 0.1[s] after the event. The placement of the slack variable is such that it can be used as a metric to see how much the vehicle intrudes into the safety zone.

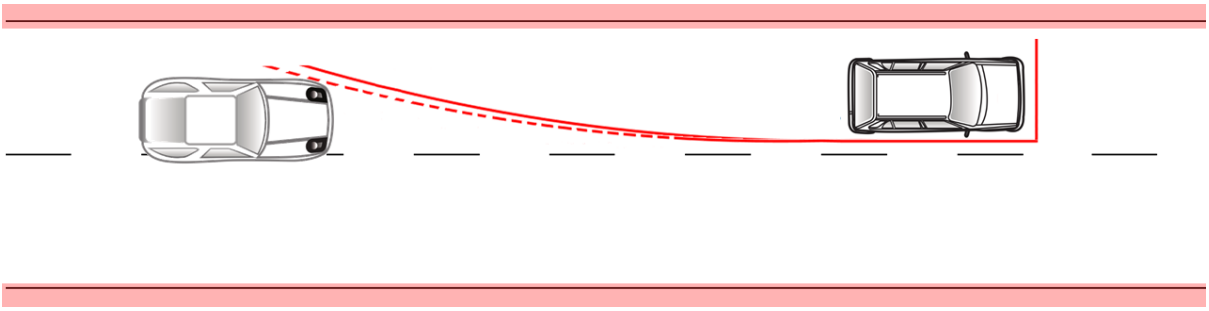

Figure 5-5: The safety zone constraint (full red line) and the 0.1[s] added on margin (dotted red line).

As the maximum expected acceleration from the rear is orders of magnitude lower than the expected deceleration in the front, the necessary margin in the rear is negligible and therefore left out. Equations (5-44) and (5-45) describe the forward-facing safety zone (when driving in front of another vehicle) for vehicles in the left and right lane respectively.

$$\frac{1}{2}a_{y,max} \cdot (\mathbf{TTC_{rear,i}})^2 - y_{ego} + y_i - \frac{1}{2}W_{ego} - \frac{1}{2}W_i \geq \zeta_i \quad (5\text{-}44)$$

$$\frac{1}{2}a_{y,max} \cdot (\mathbf{TTC_{rear,j}})^2 + y_{ego} - y_j + \frac{1}{2}W_{ego} + \frac{1}{2}W_j \geq \zeta_j \quad (5\text{-}45)$$

Here $TTC_{trail,i}$ and $TTC_{trail,j}$ are both described by equation (4-7) in Chapter 4 and the values for $x(t)$ are filled in using the state predictions from step 2.

In the optimisation all safety constraints for front- and rear-facing safety zones are implemented on all the surrounding vehicles, in the case of this thesis that means $n + m = 3$ vehicles, thus 6 constraints in total. There are however a maximum of 3 active constraints, as a vehicle can only have the front- or the rear-facing constraint activated. To activate the constraints the communicated state trajectories $\mathbf{x(t)}$ are used. These are communicated between the solver

steps as a series of parameters, and depending on whether the constraint should be active or not; the communicated value for $x(t)$ is appended to a very high value. Listing (5.1) shows an example of how the state trajectories used in the constraints are appended.

```
for i = 1:N
    if x_data(i) < (x1traj(i)+0.5*LE+0.5*LO)
        x_front(i) = 9999;
        x_rear(i) = x_data(i);
    else
        x_front(i) = x_data(i);
        x_rear(i) = 9999;
    end
end
```

Listing 5.1: Example of code used to active either the front-facing or rear-facing safety zone constraint on a specific vehicle.

Now that the inequality, state and input constraints have been defined, the OCP is formulated using equations (5-46) to (5-49), with the set of vehicles states $\mathcal{X}$ and controls $\mathcal{U}$ governed by model equations (5-31) to (5-33).

$$\mathcal{X} = [y, \psi, \delta, \dot{\delta}] \tag{5-46}$$

$$\mathcal{Y} = [y, \psi] \tag{5-47}$$

$$\mathcal{U} = [\ddot{\delta}, \zeta_1, \zeta_2, \zeta_3] \tag{5-48}$$

$$\begin{aligned} OCP &= \min_{\mathcal{Y},\mathcal{U}} \int_{t=0}^{t_f} \left((\mathcal{Y} - \mathcal{Y}_{ref})^2 + \mathcal{U}^2\right) dt \\ &= \min \int_{t=0}^{t_f} \left(K_{14}\ddot{\delta}^2 + K_{15}\psi^2 + K_{16}a_y^2 + K_{17}(y - y_{ref})^2 + K_{18}\zeta_1^2 + K_{19}\zeta_2^2 + K_{20}\zeta_3^2\right) dt \end{aligned} \tag{5-49}$$

The cost function, equation (5-49) is set up to minimize the difference between the vehicle's lateral position and the reference, thus finding the point of maximum lateral intrusion. Further quadratic costs are included on $\ddot{\delta}, \psi$ and a_y to minimize control effort, and penalize lateral acceleration to create a comfortable trajectory. K_{14} to K_{20} provide once again the cost weights used as tuning parameters, divided in two sets for nominal driving and evasion maneuvers respectively.

The solution to this OCP will result in the lateral part of the path, $[y, \psi, \delta]$, which together with the longitudinal trajectories from step 2, $[x, v_x]$, form the complete path to be followed by the vehicle, conforming with all of the (safety zone) constraints optimized towards the defined objectives.

Chapter 6

Real-Time Implementation

6-1 Real-Time

In recent years the real-time implementation of Nonlinear Model Predictive Control (NMPC) has seen an uplift with the development of frameworks, structure exploitations and feedback schemes[17][18][19]. Two tools in particular, ACADO and FORCESPro, provide problem-tailored auto-generated C-code solvers allow many new problems to be tackled. The former uses a Sequential Quadratic Programming (SQP)-approach, while the latter, the tool used in this thesis, is based on Interior Point Methods (IPM).

6-2 Interior Point Methods

The main key to any Newton-type method to solve a nonlinear program, are the Karush-Kuhn-Tucker (KKT) conditions for optimality (equations (6-1) to (6-5)). Any solution for which there exists a μ and λ that satisfy these equations, is a (locally) optimal solution[20].

$$\nabla J(x) + \nabla g(x)\lambda + \nabla h(x)\mu = 0 \tag{6-1}$$
$$h(x) = 0 \tag{6-2}$$
$$g(x) \leq 0 \tag{6-3}$$
$$g(x)\lambda = 0 \tag{6-4}$$
$$\lambda \geq 0 \tag{6-5}$$

There are two main approaches to solve this set of equations, SQP and IPM.

In SQP all nonlinear equations appearing in the dynamics $f(x)$ and constraints $g(x)$ and $h(x)$ are linearized, resulting in a convex Quadratic Program (QP) of which solutions can reliably found.

The second approach and the one of interest here, is the class of IPM. In this framework the inequality constraints $g(x)$ are relaxed with a penalty τ, replacing equations (6-3) to (6-5) with a new relaxed version in equation (6-6).

$$g(x)\lambda = \tau \tag{6-6}$$
$$\tau > 0 \tag{6-7}$$

Solving this system using Newton's method leads to a solution of the problem in equations (6-8) to (6-10) [18].

$$\min_x J(x) - \tau \log(-g(x)) \tag{6-8}$$
$$\text{s.t.} \tag{6-9}$$
$$h(x) = 0 \tag{6-10}$$

Here the original cost function is adapted with a barrier function based on the inequality constraints, which means the solution lies in the interior set described by those constraints. The penalty τ can then be reduced and the system can be solved again. Reducing τ by a fixed step in every iteration will lead to the solution of the original NLP as τ approaches 0.[21]

6-3 FORCES Pro

FORCES Pro is a commercial nonlinear interior point solver based on the FORCES solver developed by Embotech. It employs IPM for non-linear proramming, in combination with a structure-exploiting linear solver it can achieve computation times in the range of typical QP-solvers[22].

In comparison to the ACADO-toolbox which delivers approximate solutions to the optimal control problem, ForcesPRO delivers solutions much closer to the optimal solution (comparable to those calculated with IPOPT for example) while only being slightly slower than the first-mentioned. Furthermore Embotech is working on ISO26262 certification allowing the future use in automotive applications, making it a more attractive solution to Volvo Cars / Zenuity than the open-source program ACADO.

In order to solve the nonlinear program outlined in equation (5-11) it needs to be discretized. Using the built-in `continuous_dynamics` functionality of FORCES Pro, the continuous dynamics can be defined and discretized using CASADi with a explicit Runge-Kutta integrator. This way the dynamical equations can be programmed as continuous time functions. The cost function and inequality constraint are then defined per 'stage' or prediction horizon step. This allows the implementation of the state prediction series from one of the optimisation steps as a parameter series in the next. Finally the state and inequality bounds are also defined per stage.

6-4 Solver Setup

The sampling rate was chosen at 10[Hz], meaning a discretization step of 0.1[s], with a prediction horizon of N = 50 samples. This was done as the algorithm calculation time became relatively large when using more samples, and to account for as much information as possible in the planning, all the radar data spanning ≈100[m] ahead should be used. At the speeds relevant to this thesis, around 20[m/s], this means a prediction horizon of 5[s] is needed.

Although hot-starting is not as crucial as in the Real-Time Iteration scheme[22], it does reduce the calculation time needed. Therefore the solution from each of the three optimisation problems

is used as an initial guess in the next iteration. When either the NLP-solvers in step 2 or step 3 cannot find a feasible solution, the path from step 1 is used as an initial guess for the next iteration.

To execute the solver a 2010 Dell laptop with an Intel Core i7 X940 at 2.13GHz was used, and a solution is chose as optimal when after an iteration the KKT-tolerances lie within the following margins:

$$\text{Equality Tolerance} \leq 10^{-6} \tag{6-11}$$

$$\text{Inequality Tolerance} \leq 10^{-6} \tag{6-12}$$

$$\text{Stationarity Tolerance} \leq 10^{-5} \tag{6-13}$$

This means all of the equality and inequality constraints have to lie within 10^{-6} of meeting the KKT-conditions, and the margin on the stationarity tolerance implies that the gradient is small enough to state that a (local) optimum has been found[23].

Chapter 7

Results

In this chapter, the results of the simulations using the developed path planner will be discussed. First the criteria, scenarios and simulation setup wil be introduced after which the scenarios will each be discussed in detail.

7-1 Simulation Results

In order to validate the functionality of the lane change algorithm; 4 specific scenario's were designed and simulated to high-light different aspects of the solution. The criteria on the lane change algorithm are set as follows:

1. **Criterium 1**: It should be able to change lanes and find the point of maximum lateral intrusion.
2. **Criterium 2**: It should stay outside the safety zones in order to guarantee availability of an evasion maneuver.
3. **Criterium 3**: It should be able to plan an evasion maneuver based on an event that falls within the design assumptions, whilst not exceeding the maximum lateral acceleration defined in Section 4-1 . This includes having the ability to plan paths which overtake other vehicles within the prediction horizon.
4. **Criterium 4**: It should be able to take into account safety zones on multiple vehicles, spread over multiple lanes.
5. **Criterium 5**: It should be robust towards prediction errors; specifically with regards to predictions on surrounding vehicle behaviour.

To check whether these criteria have been met, the following 4 scenarios were set up.

1. **Scenario 1**: The ego-vehicle attempts to merge between two vehicles driving at constant speed in the target lane. There is no reaction from the two vehicles to the merging maneuver. This scenario is aimed validating criterium 1 and 2, as the ego-vehicle should settle against the constraints in the gap, and at no point breach the safety zone constraints.

2. **Scenario 2**: The ego-vehicle attempts to merge between two vehicles and is let in by a yielding reaction from the trailing vehicle. While on the edge of the safety zone for the lead vehicle, it comes to a sudden stop. This scenario is aimed at validating criterium 3 and 5, as the ego-vehicle should be able to evade the lead vehicle without exceeding the pre-set maximum lateral acceleration, and should do so without prior knowdledge of the accident. Planning this evasion maneuver will also include overtaking the vehicle on the prediction horizon.
3. **Scenario 3**: The ego-vehicle attempts to merge between two higher velocity vehicles in the target lane, to overtake a vehicle in the host lane. This scenario is aimed at validating criterium 4, as the ego-vehicle should respect safety zones on vehicles in both target and host lane. It also validates part of criterium 3 as a vehicle is overtaken on the prediction horizon.
4. **Scenario 4**: The ego-vehicle attempts to merge between two higher velocity vehicles in the target lane, to overtake a vehicle in the host lane, but is cut-off by the vehicle from behind and, when collision becomes imminent, receives the command to abort the lane change. This scenario is aimed at validating criterium 4 and 5, as the ego-vehicle should respect safety zones on vehicles in both target and host lane while also being confronted with prediction error on the behaviour of the trailing vehicle.

To perform the simulation of these scenarios, the simulation framework as depicted in Figure 7-1 was used. A (simulated) perception module is set up to provide measurements on surrounding vehicle movement and road related constraints such as lane width and speed limits. On the real vehicle this would be a sensor-fusion module, creating a surroundings map from different sensor inputs. In this simulation environment the surrounding vehicle movements and environment changes are pre-mapped by the author.

The control structure relies on a higher-order decision module which provides decisions on whether to change lane or not. In the real vehicle implementation this could be a behavioural machine learned algorithm[24], which takes input from a global path planner to decide when and if to change lane, but also to abort a lane change if no reaction can be provoked from surrounding road users. As this part of the control does not lie within the scope of this thesis, this decision module is simulated by user pre-defined behaviour.

The Precomputing module then takes the information from the perception module which, together with the decision to change lane or abort lane change and the current vehicle states, are turned into constraint values and references for the MPC Path Planner.

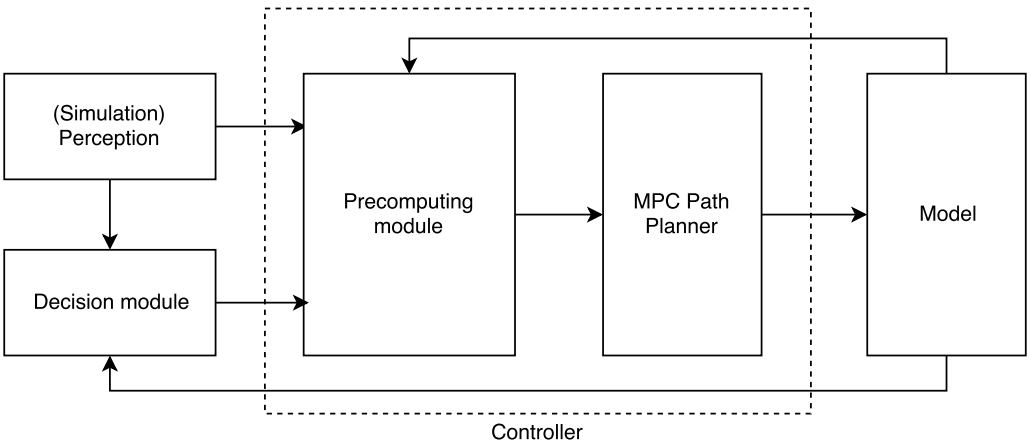

Figure 7-1: Structure of the simulation framework.

Step	Parameter	Symbol	Value Nominal	Value Evasion
1	x_{ref} weight	K_1	0.8	0
1	y_{ref} weight	K_2	50	50
1	ψ weight	K_3	0.05	0.05
1	v_{ref} weight	K_4	0	0.8
1	a_x weight	K_5	30	30
1	$\dot{\delta}$ weight	K_6	10	10
2	v_{ref} weight	K_7	0.0001	0.1
2	a_x weight	K_8	1	0.5
2	j_x weight	K_9	50	1
2	Gap finding weight	K_{10}	50	0
2	Slack 1 weight	K_{11}	100	100
2	Slack 2 weight	K_{12}	100	100
2	Slack 3 weight	K_{13}	100	100
3	$\ddot{\delta}$ weight	K_{14}	50	50
3	ψ weight	K_{15}	0.1	0.1
3	a_y weight	K_{16}	4	0.1
3	y_{ref} weight	K_{17}	5	5
3	Slack 1 weight	K_{18}	10^6	10^6
3	Slack 2 weight	K_{19}	10^6	10^6
3	Slack 3 weight	K_{20}	10^3	10^3

Table 7-1: Tuning parameters and cost weights for the 3 MPC problems.

The MPC Path Planner itself is a consecutive execution of three different solvers as presented in Chapter 5, generating a control input for the single track model used to simulate the vehicle dynamics.

To showcase the results for each of the scenario's; aside from the presentation of vehicle states and inputs, snap shots of the graphical simulation have been taken to give an impression of the algorithms functionality. In this graphical simulation, the safety zone constraint on the vehicle is shown as a red line which presents a spatial constraint, based on the ego- and surrounding vehicle states at that moment. Although in the path planner this constraint acts on the ego-vehicle center, in the graphical simulation it has been transposed to show as acting on the outer corners of the vehicle. This is for clarification purposes only, and this sometimes results in incorrect visualization far away from the ego-vehicle or at areas where constraint switching should occur (such as near or directly around another vehicle).

The results of the simulation of these scenarios will be discussed in Sections 7-2 to 7-5. The values for the tuning parameters and cost weights used as standard configuration in these scenarios can be found in Table (7-1). Table (7-2) shows the values for the vehicle parameter used, and finally all box constraint values for the three OCPs are shown in Table (7-3).

Parameter	Symbol	Value
CM to front axle	l_f	1.10 [m]
CM to rear axle	l_r	1.60 [m]
Front cornering stiffness	c_f	$2 \cdot 57000$ [N/°]
Rear cornering stiffness	c_r	$2 \cdot 47000$ [N/°]
Vehicle mass	m	1600 [kg]
Outside vehicle length	L_{ego}/L_i	5 [m]
Outside vehicle width	W_{ego}/W_i	2 [m]

Table 7-2: Parameters used for vehicle model and safety zone.

Parameter	Symbol	Value
Upper lane boundary	y_{max}	8 [m]
Lower lane boundary	y_{min}	0 [m]
Maximum steering angle	δ_{max}	0.75 [rad]
Minimum steering angle	δ_{min}	-0.75 [rad]
Maximum steering rate	$\dot{\delta}_{max}$	2 [rad/s]
Minimum steering rate	$\dot{\delta}_{min}$	-2 [rad/s]
Maximum longitudinal acceleration	$a_{x,max}$	8 [m/s^2]
Minimum longitudinal acceleration	$a_{x,min}$	-8 [m/s^2]
Maximum longitudinal jerk	$j_{x,max}$	50 [m/s^3]
Minimum longitudinal jerk	$j_{x,min}$	-50 [m/s^3]
Maximum speed	v_{max}	25 [m/s]
Dry friction limit	μ_{max}	1

Table 7-3: Values used for the box constraints on the OCPs.

7-2 Scenario 1: Lane Change without Reaction

In the first scenario, the controller is instructed by the decision module to initiate a lane change, which translates to a change of lateral reference for the MPC Path Planner. Screenshots of the ego-vehicle movement can be seen in Figure (7-2). As expected, in Figure (7-2c) it can be seen that the safety zone constraint for the lead vehicle enlarges towards the ego-vehicle when it heads into the gap. Then, as the relative heading decreases in Figure (7-2e) the safety zone constraint becomes smaller and the ego-vehicle can move further into the gap, until it is settled at maximal intrusion between the two vehicles in Figure (7-2f). This means Criterium (1) is met for this scenario.

The settling on the constraints can also be seen in Figure (7-4a) and (7-4b), as the values for the Time-To-Collision (TTC) and Avoidance-Maneuver-Time (AMT) approach each other for both trailing and leading vehicle. With regards to the lead vehicle, the AMT converges to TTC minus margin, which was added to increase robustness (see Section 5-4). The AMT never becomes larger than the TTC, meaning Criterium (2) is also met.

Furthermore the lateral acceleration as seen in Figure (7-3d), as wel as the longitudinal acceleration depicted in Figure (7-3e) remain within comfortable limits as set in Chapter 2. The steering rate input is within actuator limits as set in Table (7-3).

The slack variables on the safety zones for the trailing and leading vehicles are shown in Figure (7-4c). As the AMT for the rear vehicle never exceeds the TTC, the corresponding slack variable is always 0. As the ego-vehicle moves into the gap on the edge of the lead vehicle safety zone, the corresponding slack variable is activated to deal with the constraint violations that result from prediction error or model mismatch. However since a margin was added the real safety zone constraint is never breached.

Finally the computation time for each of the simulation steps is shown in Figure (7-4d). With a mean computation time of 35ms and a maximum of 50ms, the system is real-time feasible for the sampling time of 100ms, at least when executed on the hardware used in this thesis as described in Section (6-4).

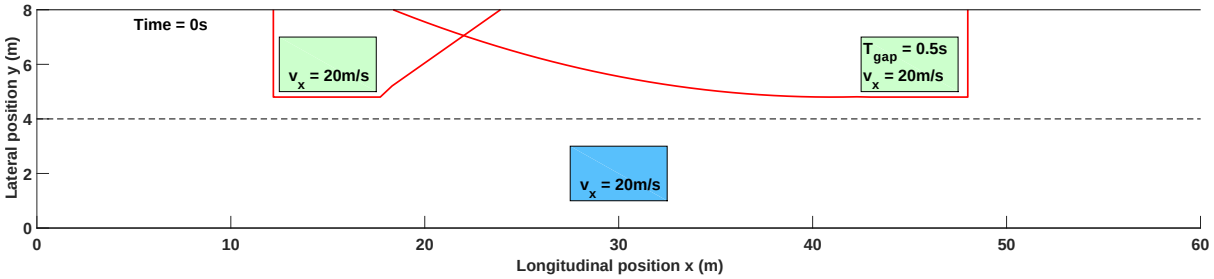

(a) Screen capture at T=0[s].

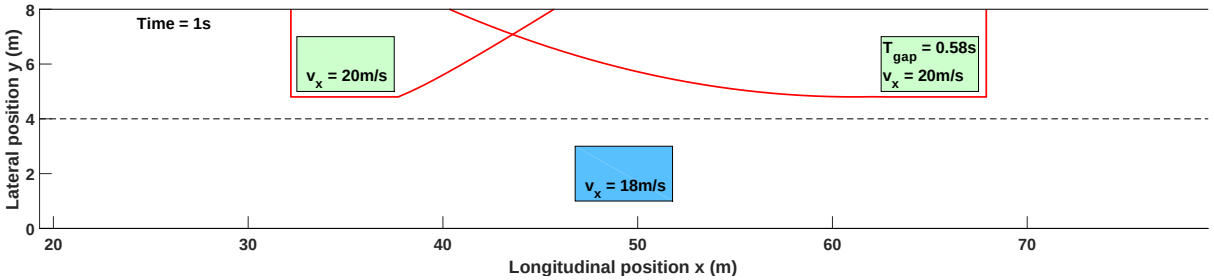

(b) Screen capture at T=1[s].

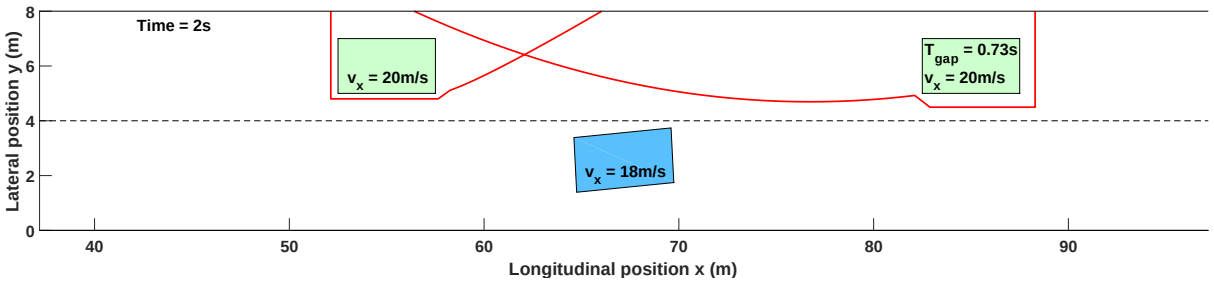

(c) Screen capture at T=2[s].

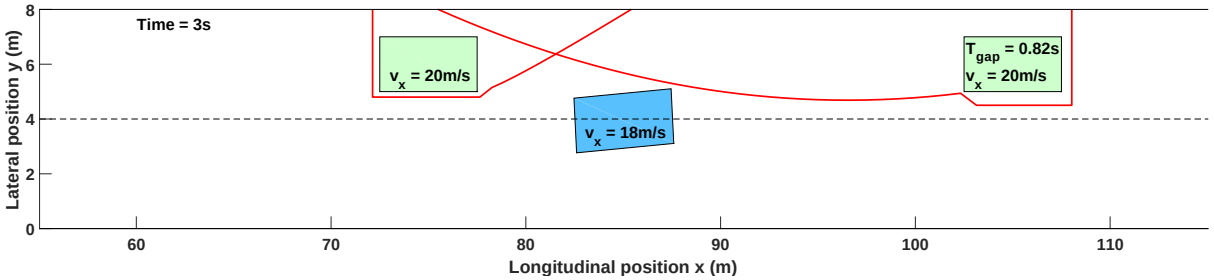

(d) Screen capture at T=3[s].

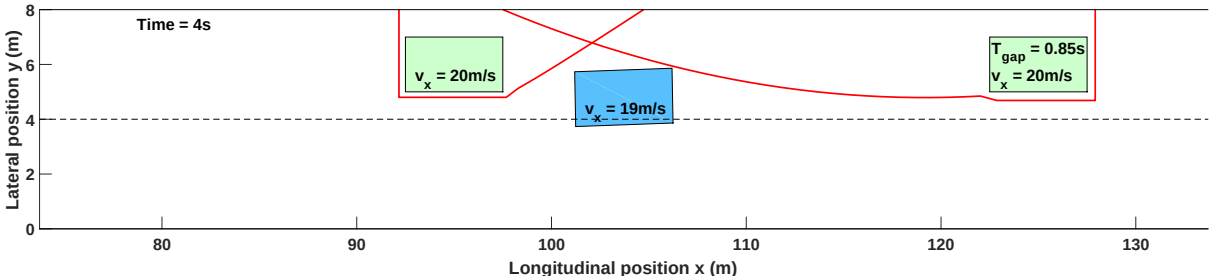

(e) Screen capture at T=4[s].

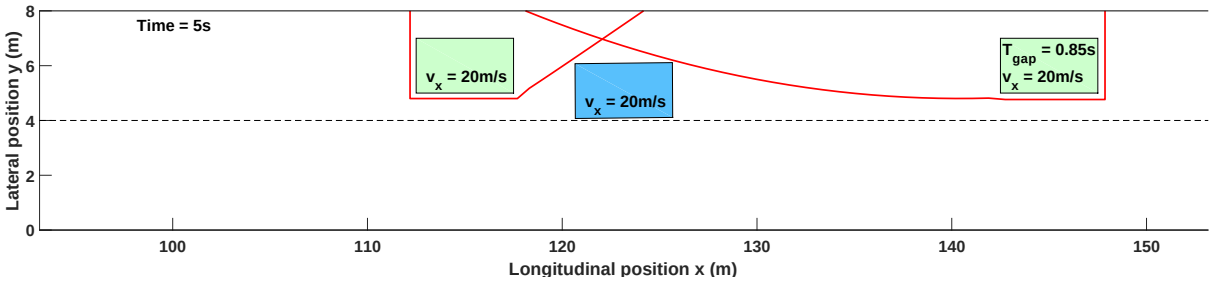

(f) Screen capture at T=5[s].

Figure 7-2: Screen captures of a simulation of scenario 1, showing a succesfull lateral intrusion by the ego-vehicle.

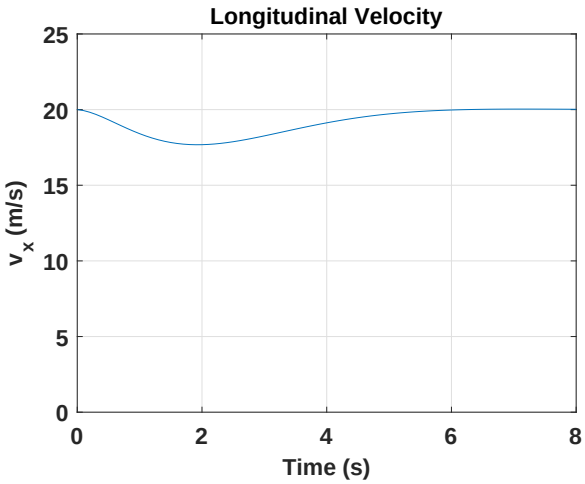

(a) Ego-vehicle longitudinal velocity v_x.

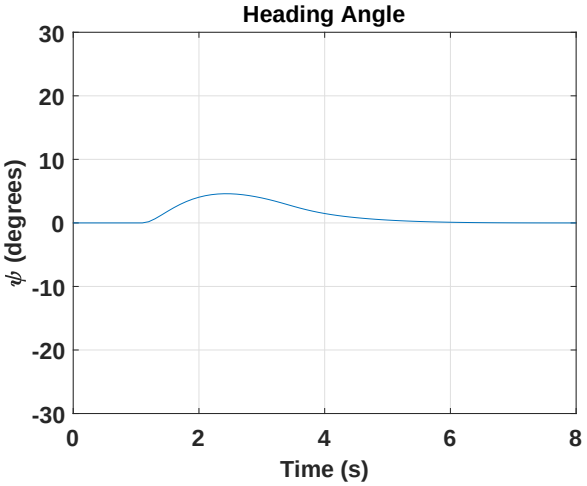

(b) Ego-vehicle heading angle ψ.

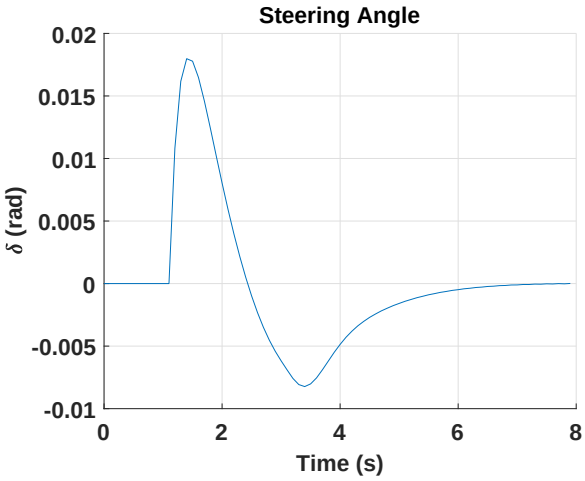

(c) Ego-vehicle steering angle δ.

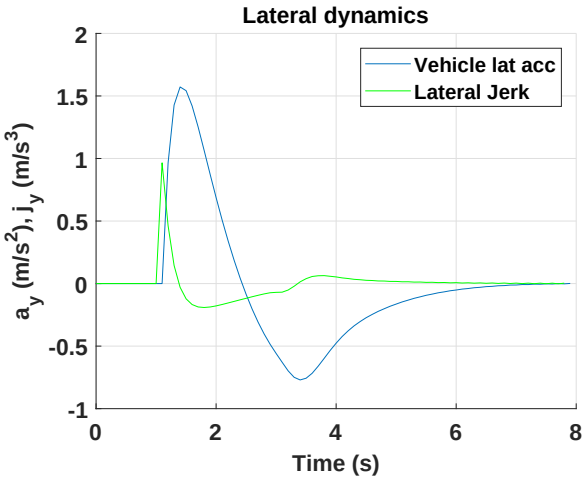

(d) Ego-vehicle lateral acceleration a_y and jerk j_y.

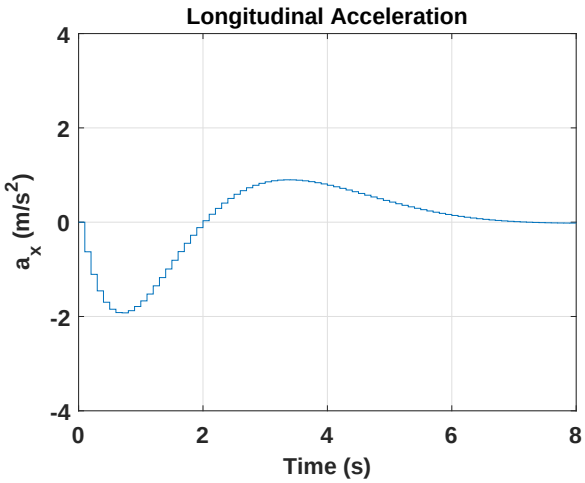

(e) Ego-vehicle longitudinal acceleration a_x.

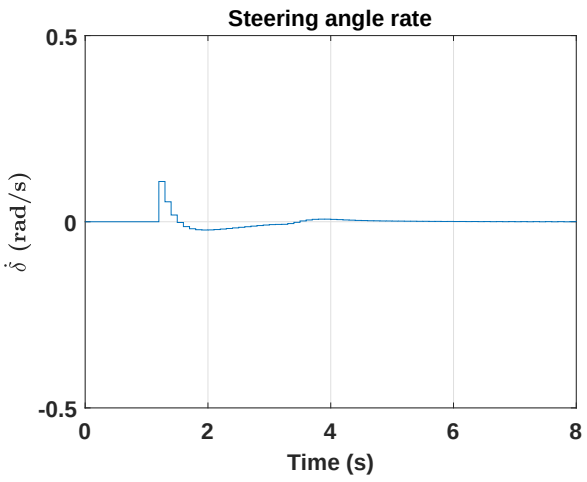

(f) Ego-vehicle steering angle rate $\dot{\delta}$.

Figure 7-3: Ego-vehicle states and control inputs for scenario 1.

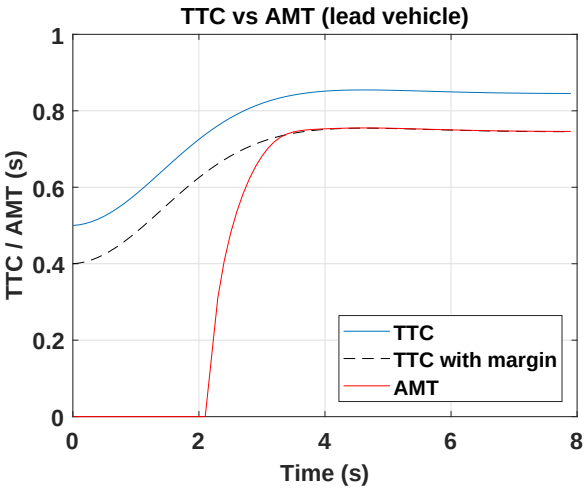

(a) Time-To-Collision and Avoidance-Maneuver-Time for vehicle 2.

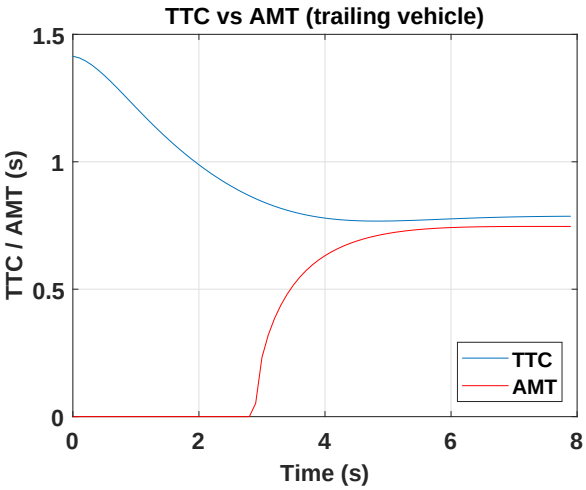

(b) Time-To-Collision and Avoidance-Maneuver-Time for vehicle 1.

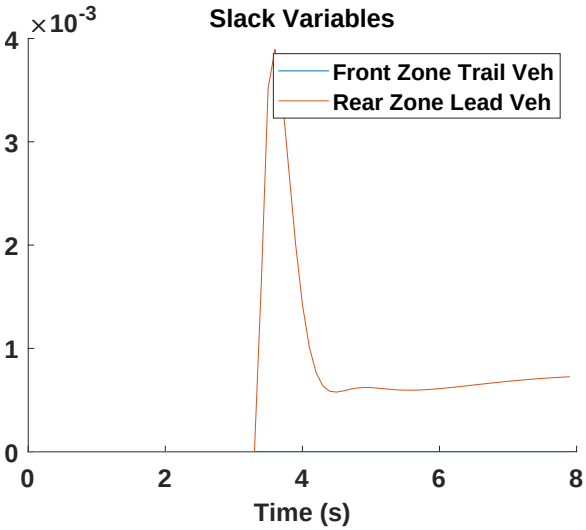

(c) Slack variable values.

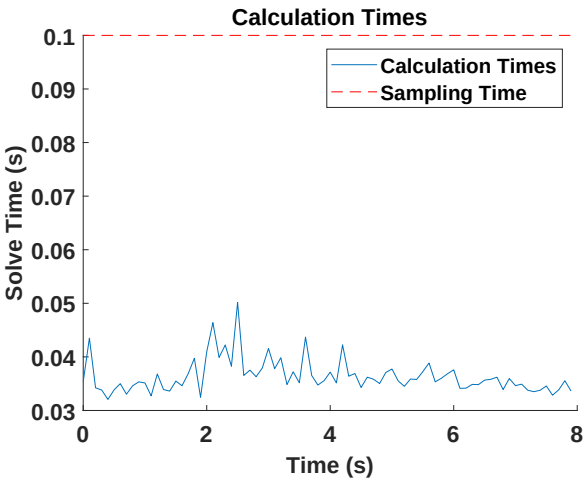

(d) Calculation times and sampling limit.

Figure 7-4: Simulation data for scenario 1.

7-3 Scenario 2: Lane Change with Evasion Maneuver

In the second scenario, the controller is again instructed to perform a lane change by change of lateral reference. The first part of the graphical simulation is similar to that in Section 7-2, the only difference being that the trailing vehicle in this scenario decelerates to let the ego-vehicle into the gap. For this reason no stills of the first part are shown in Figure (7-4). At 5.5 seconds into the simulation however, the leading vehicle comes to an instant stop. At this point the ego-vehicle is on the edge of the safety zone, and needs to perform an evasive maneuver.

Starting from Figure (7-4e) it is evident that the ego-vehicle breaches the safety zone for the first sampling time (100[ms]) after the sudden stop. The following simulation stills show how the ego-vehicle manages to return to the outside of the safety zone and perform the evasive maneuver. Looking at Figure (7-5d) reveals a minimum lateral acceleration during the maneuver of $-4.9[m/s^2]$, meaning the Criterium (3) is met as the absolute maximum allowed acceleration $|a_y|_{max}$ was $5[m/s^2]$.

When looking at Figure (7-6a) the AMT can be seen to correspond with the TTC rather well for the first part of the maneuver, but violates the constraint further into the evasion maneuver. After careful consideration, the author of this thesis found out that this is because the lateral speed is not represented in the safety zone formulations. Even though the ego-vehicle is already reducing lateral acceleration, it is still able to finish the evasion maneuver because of its built up lateral velocity.

The breach of the safety zone can also be seen in Figure (7-6c), as after $T \approx 6[s]$ in the simulation the slack variable exceeds the $0.1[s]$ threshold with a large margin. In order to retain a feasible solution however this exceedance is allowed at a high penalty.

Finally the computation time for each of the simulation steps is shown in Figure (7-6b). With a mean computation time of 35[ms] and a maximum of 44[ms], this scenario is real-time feasible for the sampling time of 100[ms], at least when executed on the hardware used in this thesis.

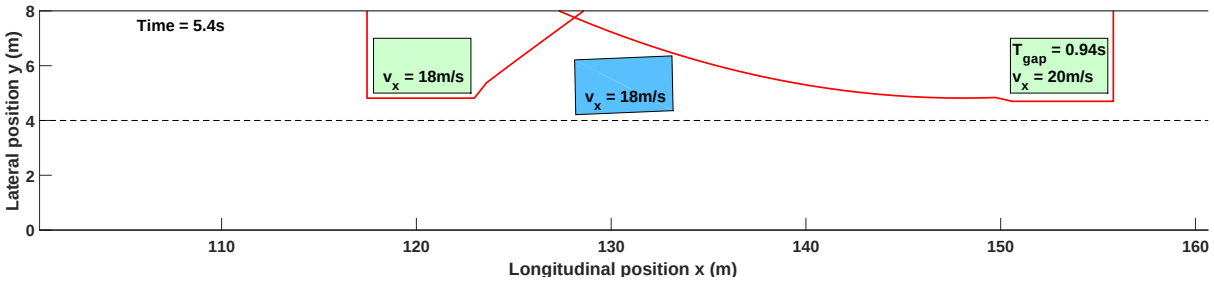

(e) Screen capture at T=5.4[s].

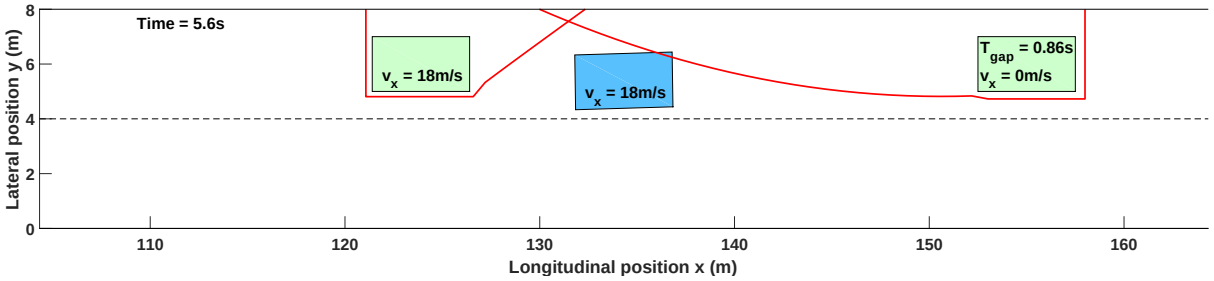

(f) Screen capture at T=5.5[s].

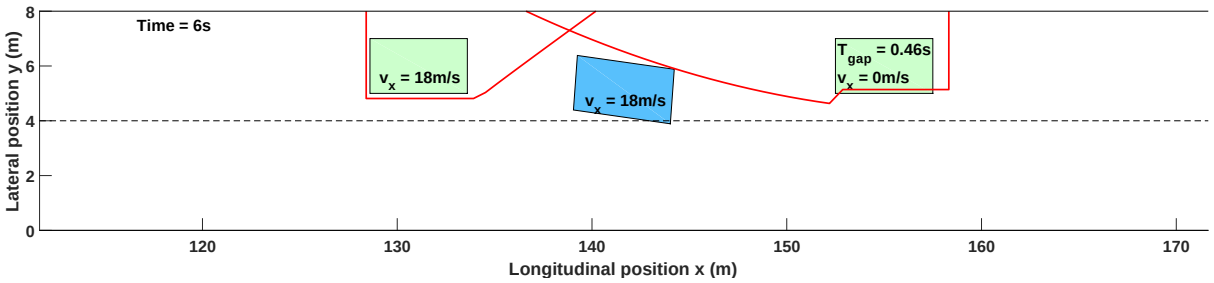

(g) Screen capture at T=6[s].

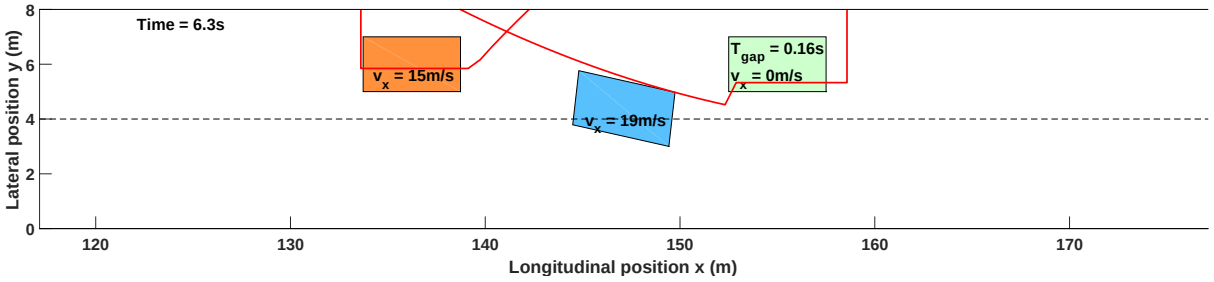

(h) Screen capture at T=6.3[s].

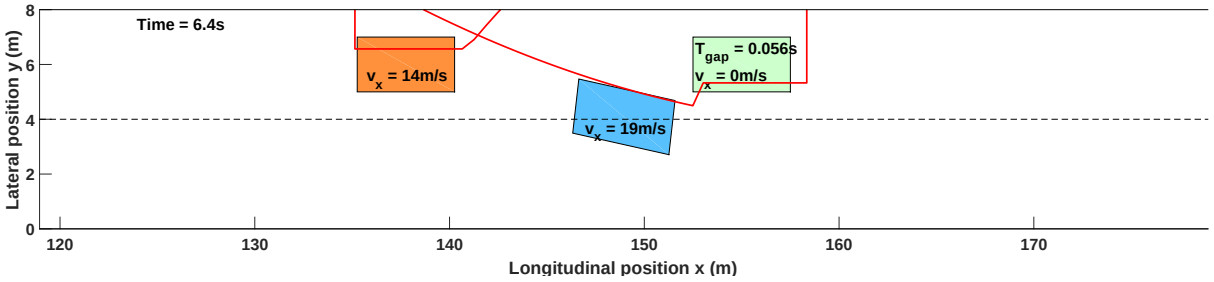

(i) Screen capture at T=6.4[s].

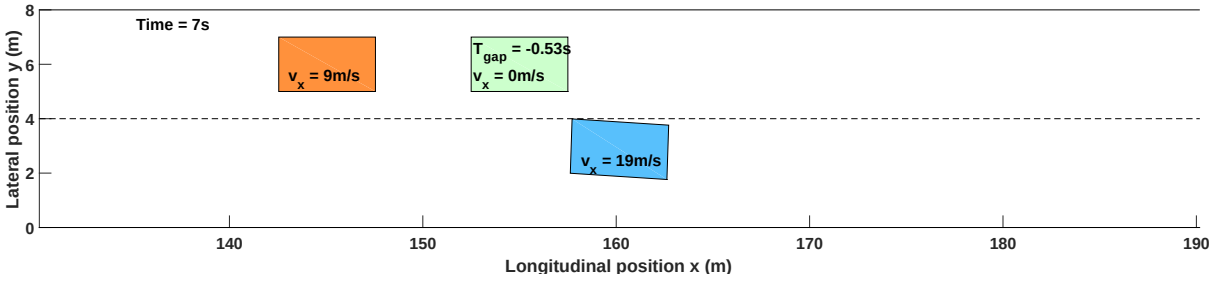

(j) Screen capture at T=7[s].

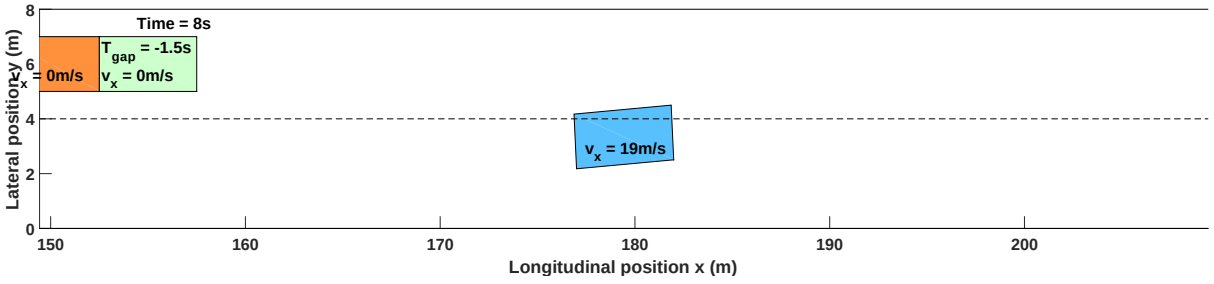

(k) Screen capture at T=8[s].

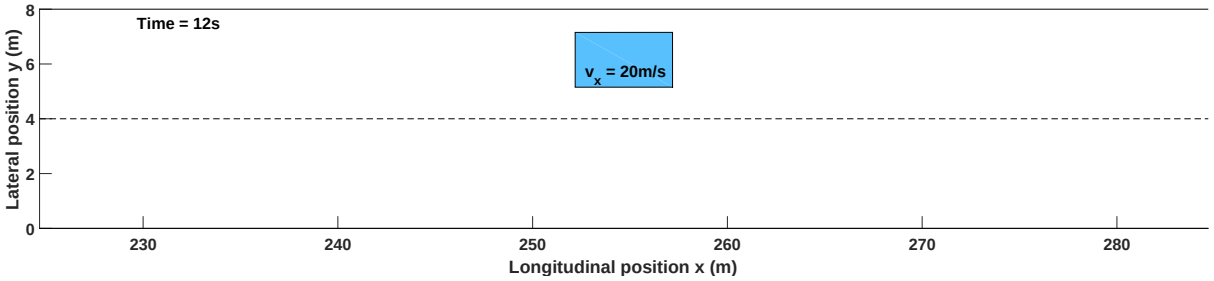

(l) Screen capture at T=12[s].

Figure 7-4: Screen captures of a simulation of scenario 2, showing a succesfull evasion maneuver by the ego-vehicle.

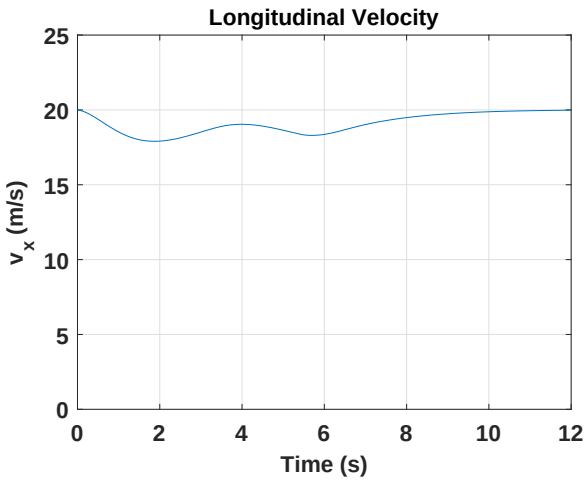

(a) Ego-vehicle longitudinal velocity v_x.

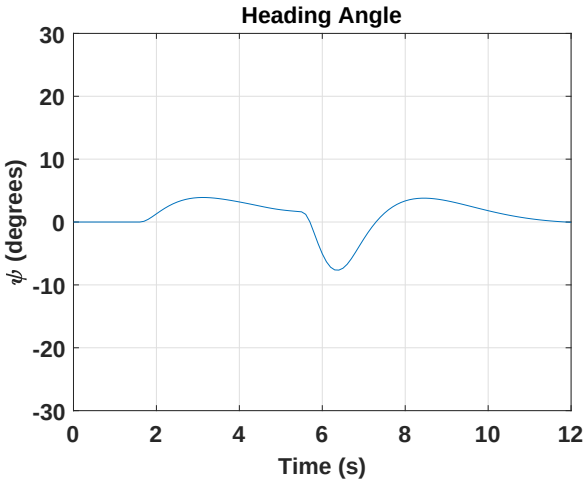

(b) Ego-vehicle heading angle ψ.

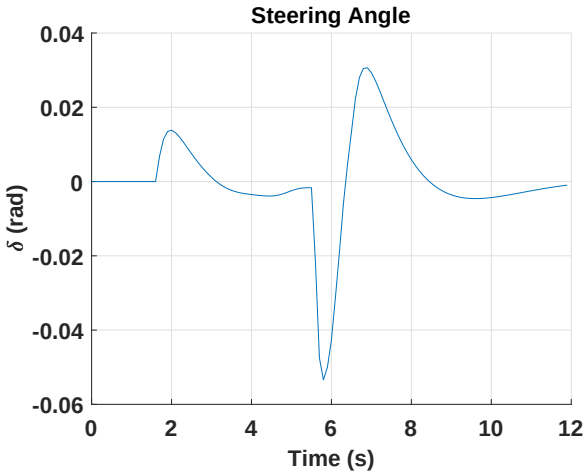

(c) Ego-vehicle steering angle δ.

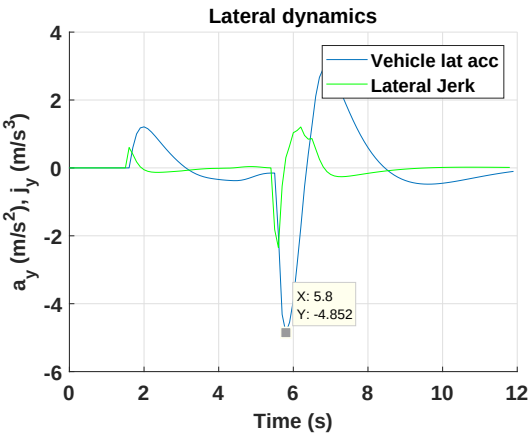

(d) Ego-vehicle lateral acceleration a_y and jerk j_y.

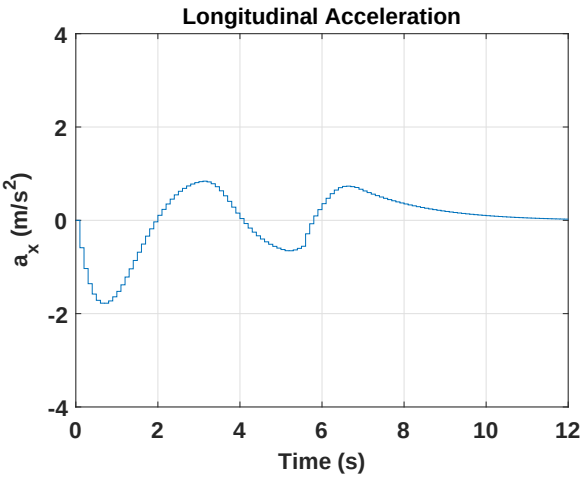

(e) Ego-vehicle longitudinal acceleration a_x.

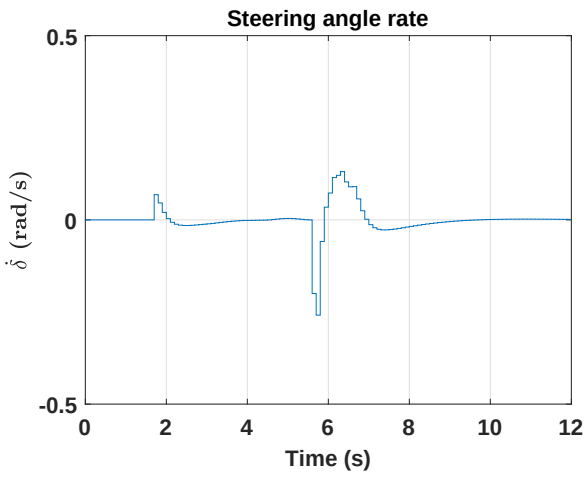

(f) Ego-vehicle steering angle rate $\dot{\delta}$.

Figure 7-5: Ego-vehicle states and control inputs for scenario 2.

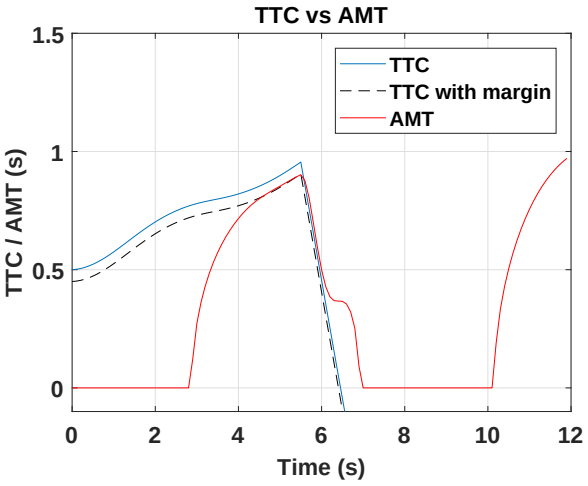

(a) Time-To-Collision and Avoidance-Maneuver-Time for vehicle 2.

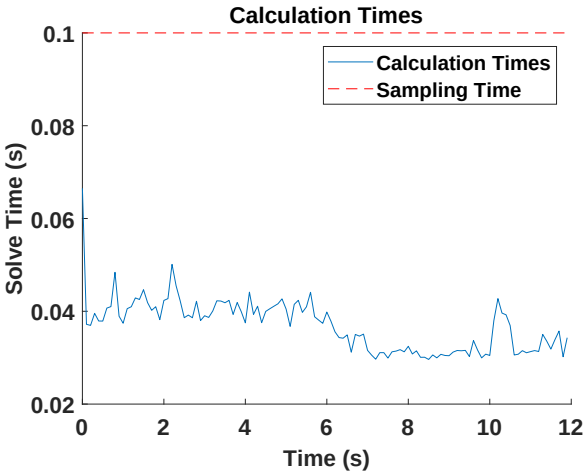

(b) Calculation times and sampling limit.

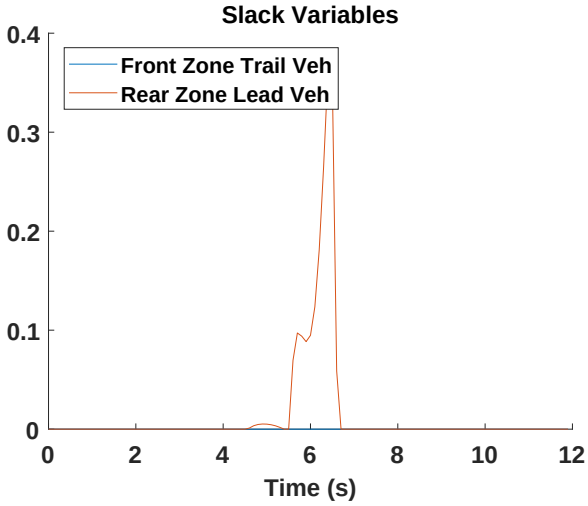

(c) Slack variable values.

Figure 7-6: Simulation data for scenario 2.

7-4 Scenario 3: Lane Change Between Multiple Vehicles

In the third scenario, the ego-vehicle finds itself travelling at 20 [m/s] in the host lane, with a slower vehicle driving 15 [m/s] in front of it. In the target lane two vehicles are driving at 20 [m/s]. The controller is instructed to change lane and merge between the two faster vehicles in the target lane to overtake the slower driving vehicle in the host lane.

At T = 1[s] the ego-vehicle comes in contact with the safety zone of the leading vehicle in the slow lane (vehicle 3), as can be seen from Figure (7-9a) as well. It is then instructed to change lane by the decision module, and moves into the gap as depicted by Figure (7-7c) to (7-7e), switching from driving on the safety zones constraint for vehicle 3 to that of vehicle 2 (leading vehicle in the target lane). This switching is again witnessed by the TTC graphs in Figure (7-9a) and (7-9b). The trailing vehicle in the target lane then decelerates to allow the ego-vehicle into the lane. The ego-vehicle has passed the lane markings before its evasion maneuver is cut-off by the slow vehicle in the host lane, and therefore the maneuver is not aborted by the decision module.

From Figure (7-9a) and (7-9b) it is evident that the relevant safety zones towards the leading vehicles in both lanes are respected, which validates Criterium (4) for this scenario. Again in Figure (7-9d) some activation of the slack variables is visible when the ego-vehicle comes in contact with the safety zone. This breach is however very small so it has no meaningfull effect on the safety of the situation, but does help to smoothen the control input, as less harsh control reaction is therefore required to keep the vehicle on the edge of the constraint.

For scenario 3 as well as the earlier scenarios, the calculation times in Figure (7-9c) confirm the real-time feasibility of the system, with a mean computation time of 35[ms] and a maximum of 63[ms].

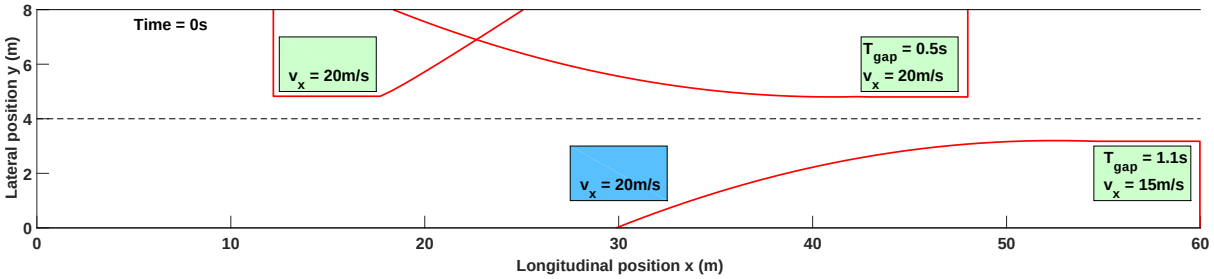

(a) Screen capture at T=0[s].

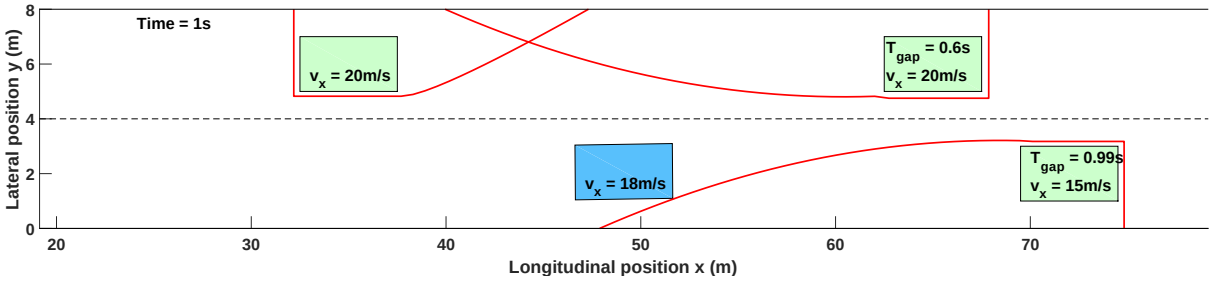

(b) Screen capture at T=1[s].

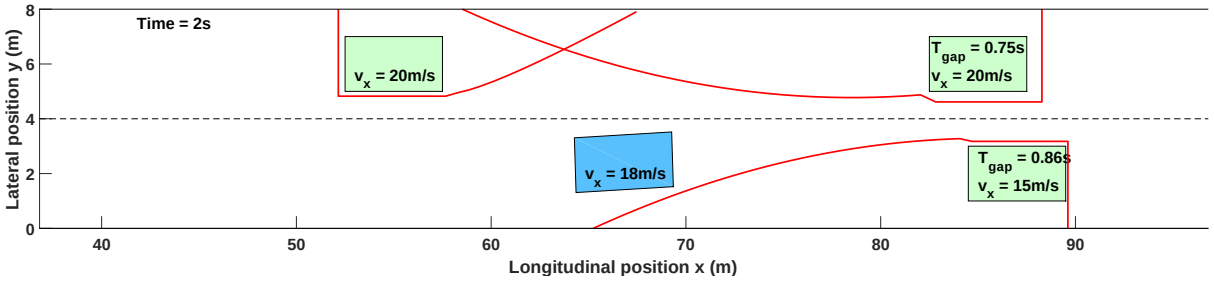

(c) Screen capture at T=2[s].

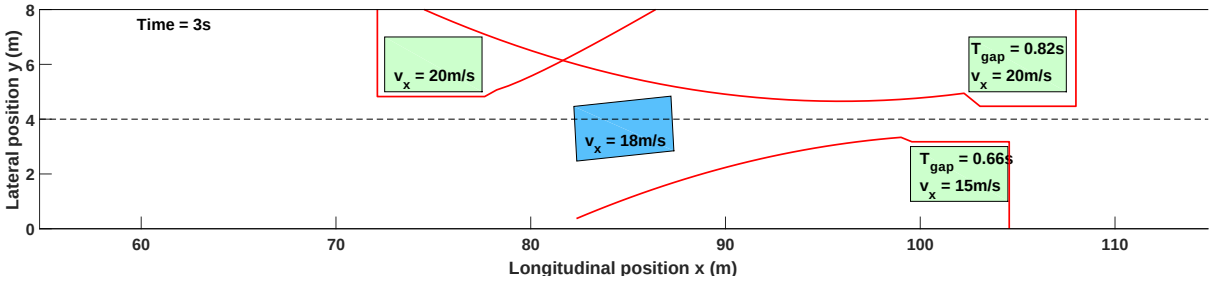

(d) Screen capture at T=3[s].

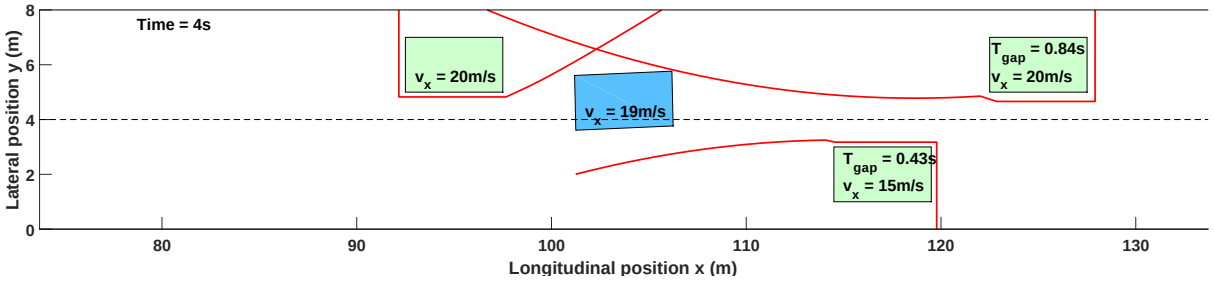

(e) Screen capture at T=4[s].

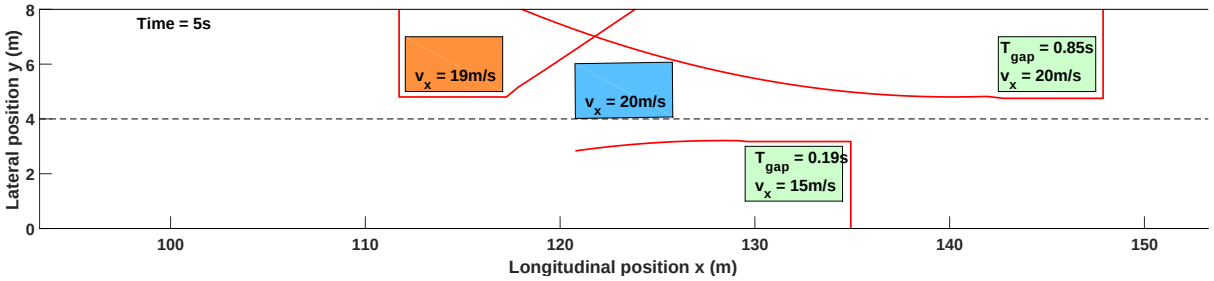

(f) Screen capture at T=5[s].

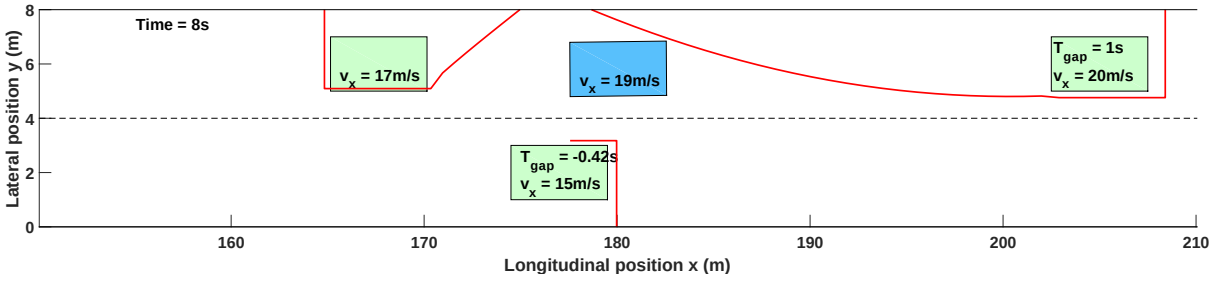

(g) Screen capture at T=8[s].

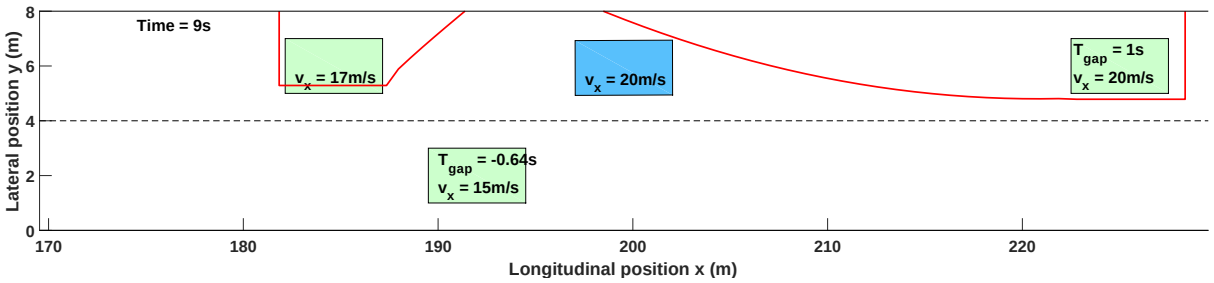

(h) Screen capture at T=9[s].

Figure 7-7: Screen captures of a simulation of scenario 3, showing a succesfull overtake and merge by the ego-vehicle.

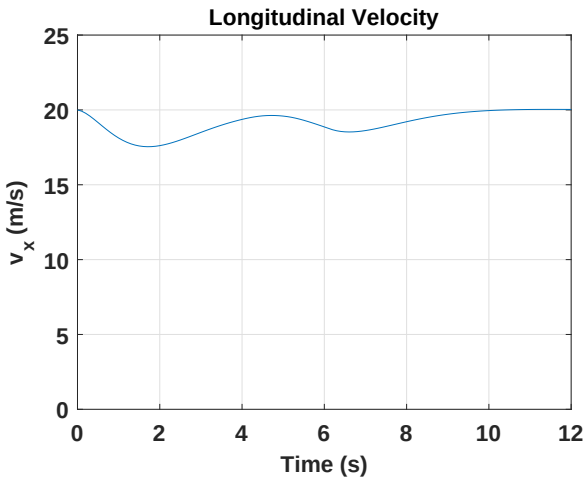

(a) Ego-vehicle longitudinal velocity v_x.

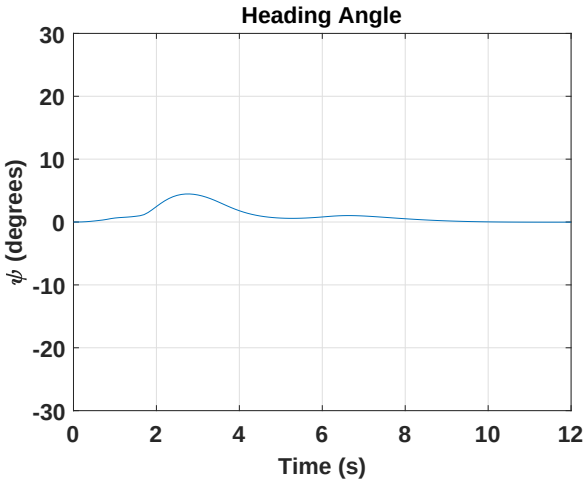

(b) Ego-vehicle heading angle ψ.

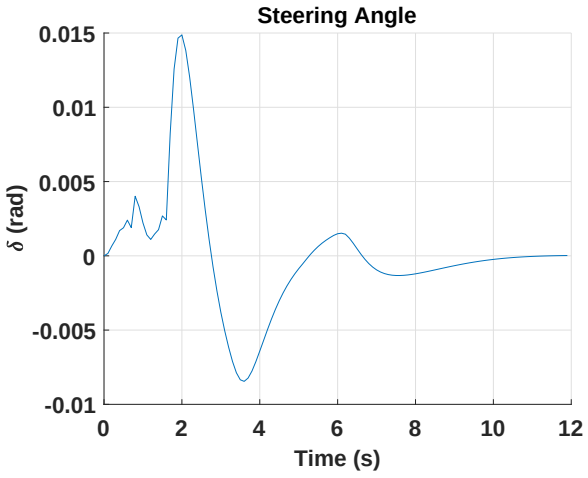

(c) Ego-vehicle steering angle δ.

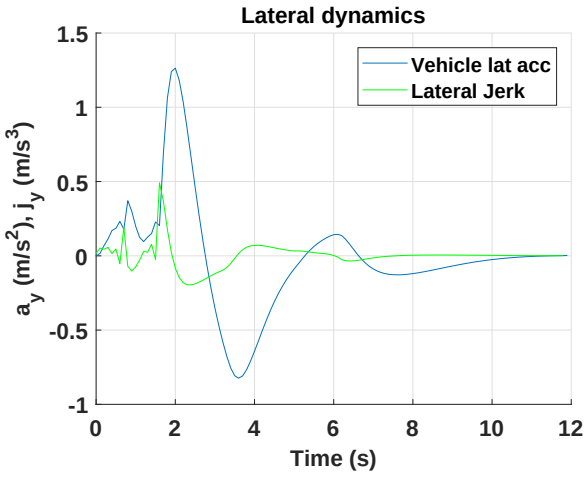

(d) Ego-vehicle lateral acceleration a_y and jerk j_y.

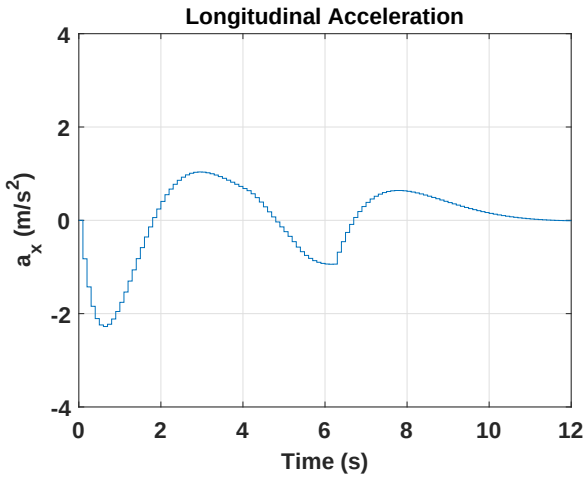

(e) Ego-vehicle longitudinal acceleration a_x.

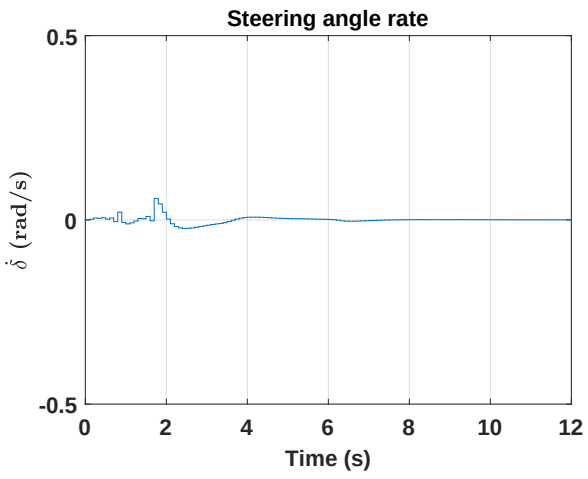

(f) Ego-vehicle steering angle rate $\dot{\delta}$.

Figure 7-8: Ego-vehicle states and control inputs for scenario 3.

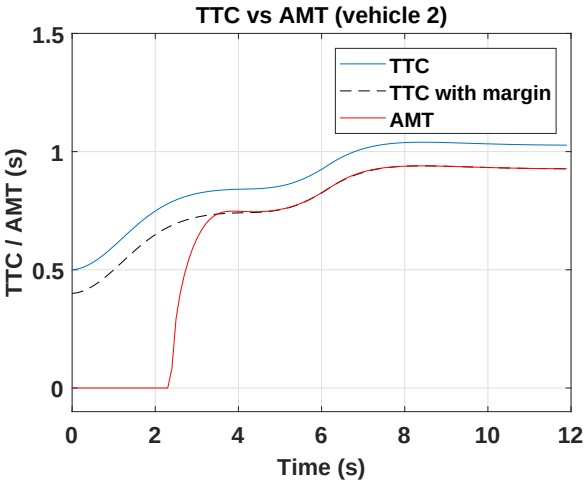

(a) Time-To-Collision and Avoidance-Maneuver-Time for vehicle 2.

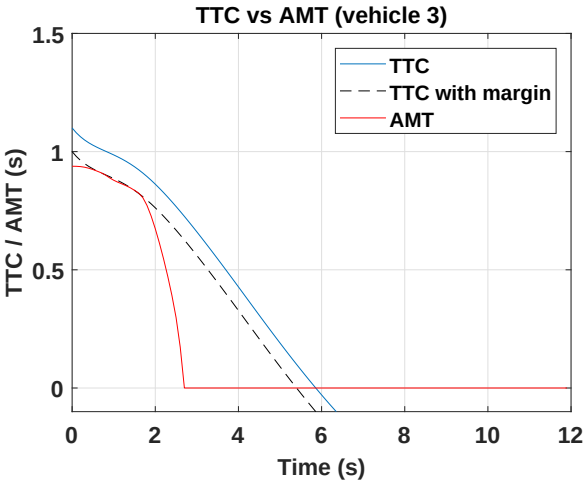

(b) Time-To-Collision and Avoidance-Maneuver-Time for vehicle 3.

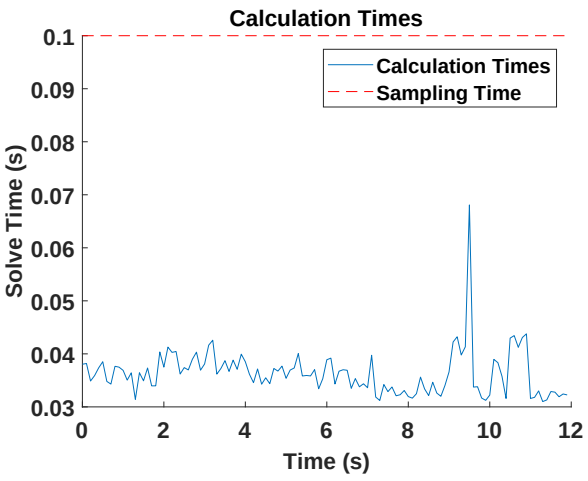

(c) Calculation times and sampling limit.

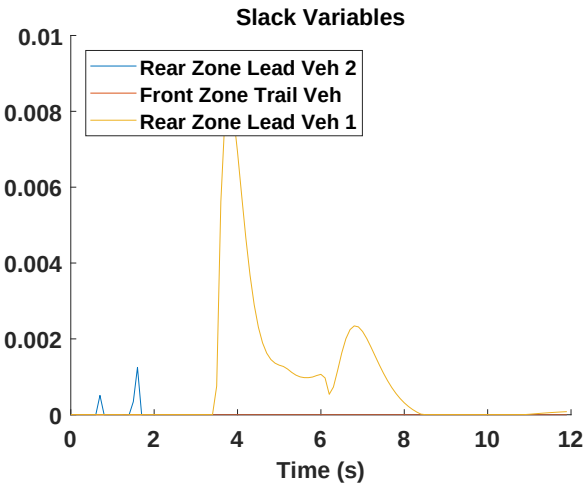

(d) Slack variable values.

Figure 7-9: Simulation data for scenario 3.

7-5 Scenario 4: Lane Change with Cut-off

In the fourth and last scenario, the ego-vehicle starts out just as in scenario 3. It is travelling at 20 [m/s] in the host lane, with a slower vehicle driving 15 [m/s] in front of it. In the target lane two vehicles are driving at 20 [m/s]. The controller again is instructed to change lane and merge between the two faster vehicles in the target lane to overtake the slower driving vehicle in the host lane. This time however, the trailing vehicle in the target lane does not yield but instead tries to cut off the ego-vehicle by accelerating.

In Figure (7-10d) to (7-10f) it can be seen that by accelerating, vehicle 1 (the trailing vehicle in the target lane) pushes the ego-vehicle forward and out of the gap. As the objective (the lateral lane reference) is still in the gap, the controller tries to stay on the point of maximum lateral intrusion. After T = 5s, the decision module issues the command to abort the lane change, so the ego-vehicle moves back to the host lane and brakes to stay outside the safety zone of the slower vehicle.

As can be seen in Figures (7-9a) to (7-4b), the TTC towards all vehicles involved in this scenario remains larger than the AMT during the relevant interactions with these vehicles. Furthermore the controller can deal with the unpredicted reaction of the trailing vehicle, so for this scenario, both Criteria (4) and (5) are validated.

Finally the computation times are shown in Figure (7-12e), and with a mean computation time of 34[ms] and a maximum peak of 57[ms] the calculation time remains smaller than the sampling time by a reasonable margin, again confirming the algorithm is real-time feasible.

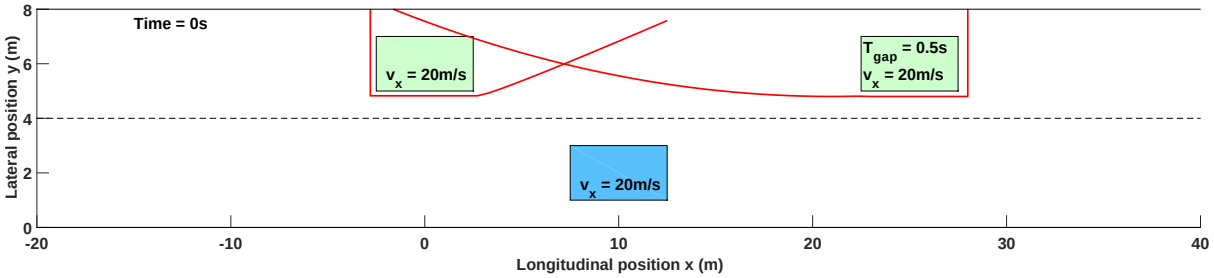

(a) Screen capture at T=0[s].

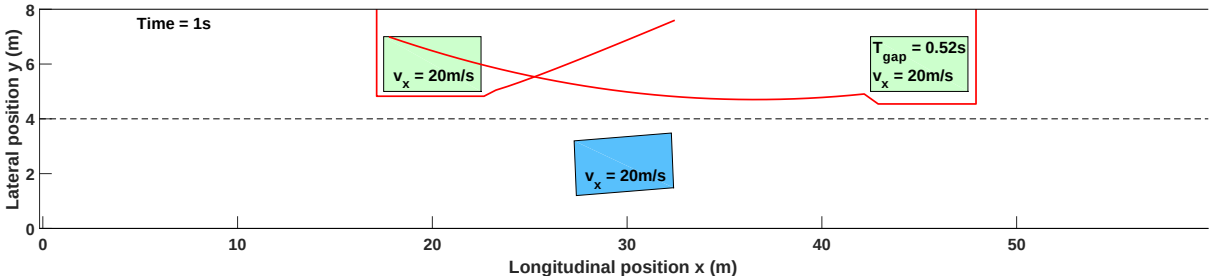

(b) Screen capture at T=1[s].

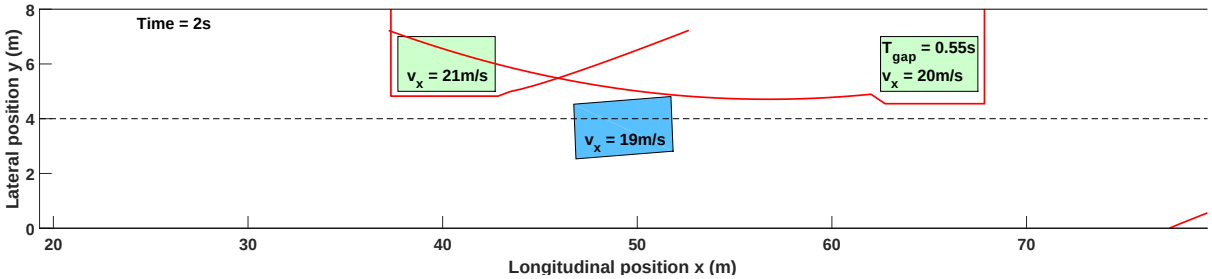

(c) Screen capture at T=2[s].

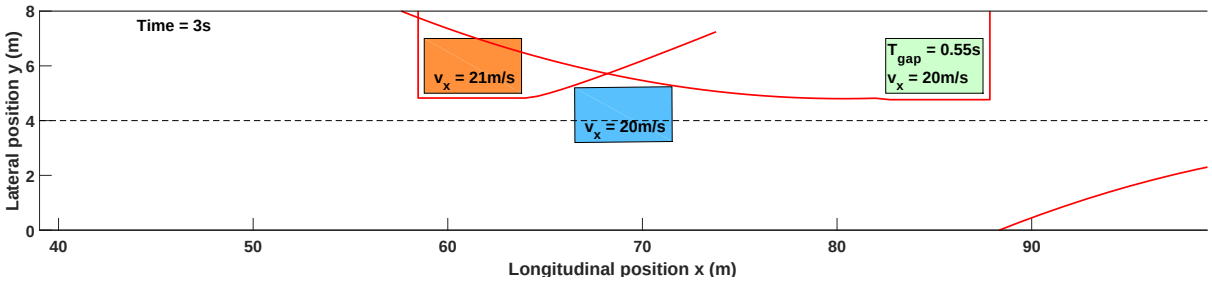

(d) Screen capture at T=3[s].

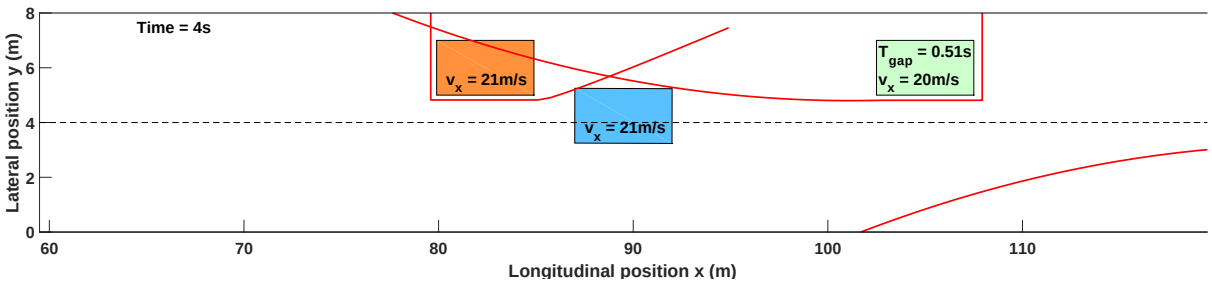

(e) Screen capture at T=4[s].

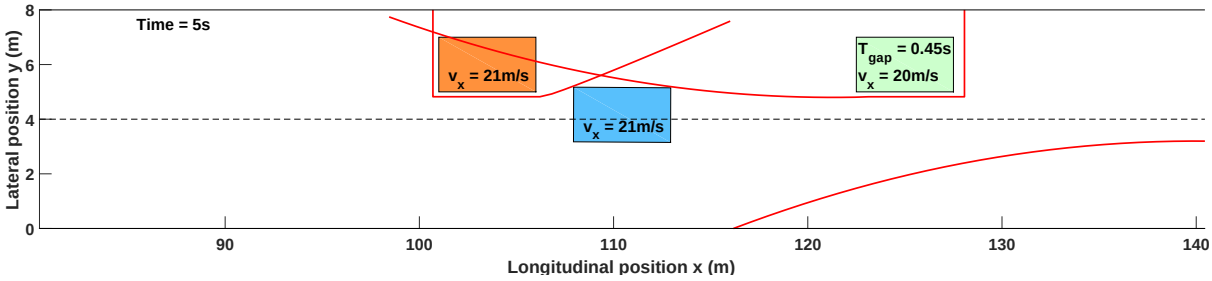

(f) Screen capture at T=5[s].

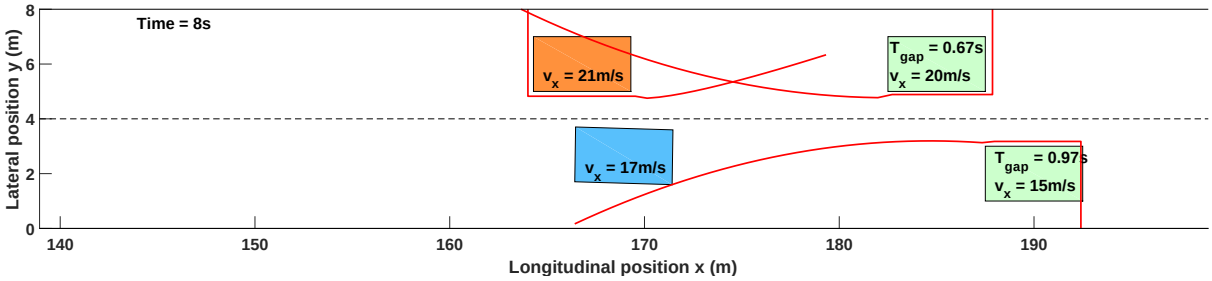

(g) Screen capture at T=8[s].

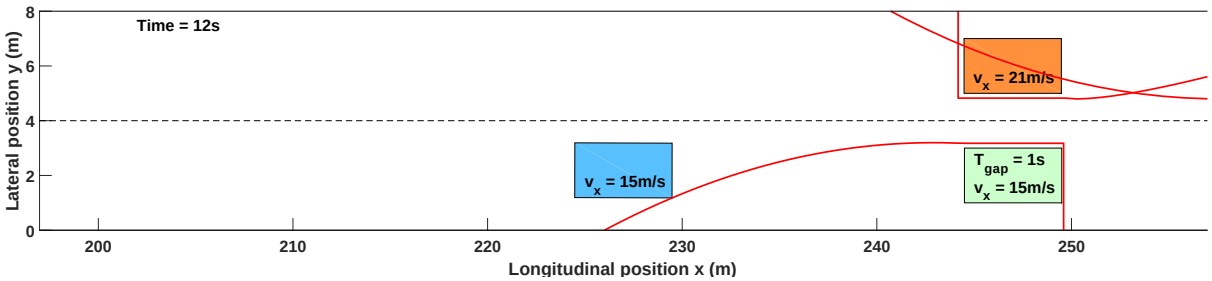

(h) Screen capture at T=12[s].

Figure 7-10: Screen captures of a simulation of scenario 4, showing a unsuccesfull merge and subsequent abort-maneuver by the ego-vehicle.

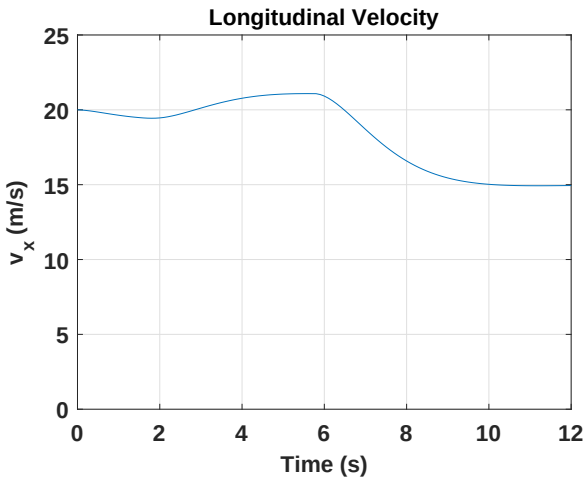

(a) Ego-vehicle longitudinal velocity v_x.

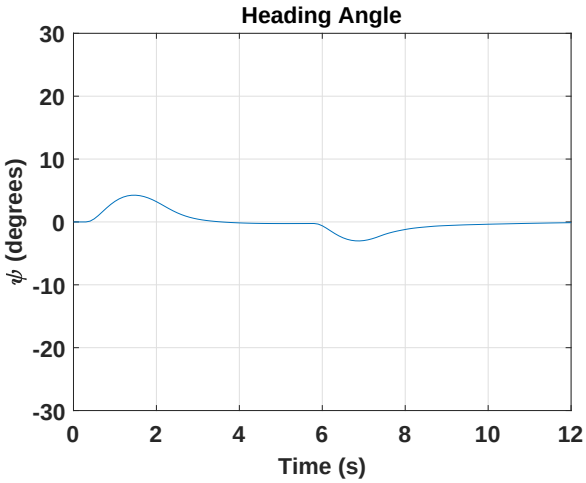

(b) Ego-vehicle heading angle ψ.

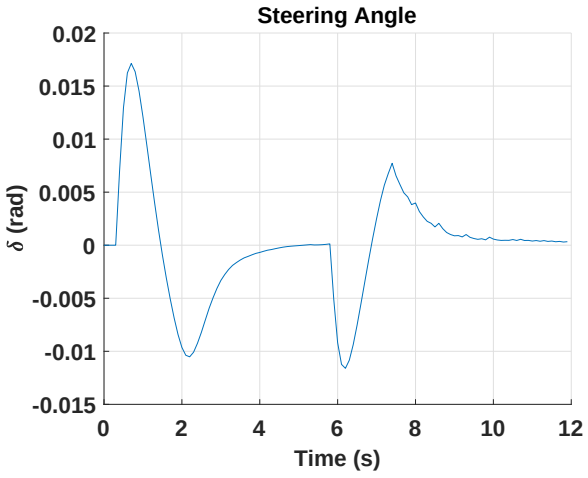

(c) Ego-vehicle steering angle δ.

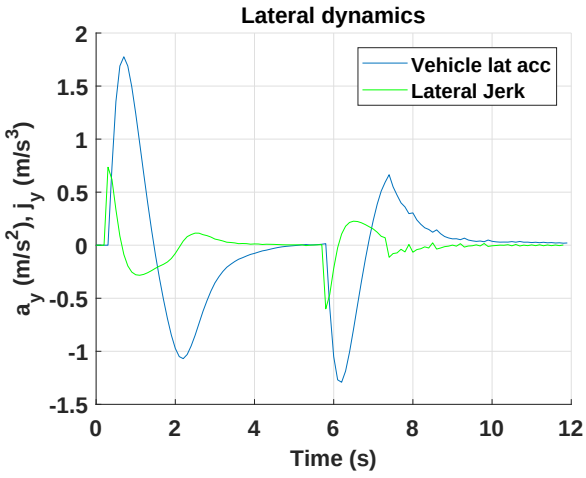

(d) Ego-vehicle lateral acceleration a_y and jerk j_y.

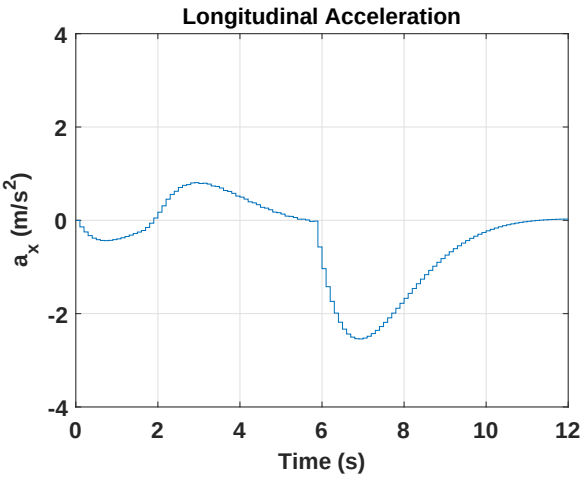

(e) Ego-vehicle longitudinal acceleration a_x.

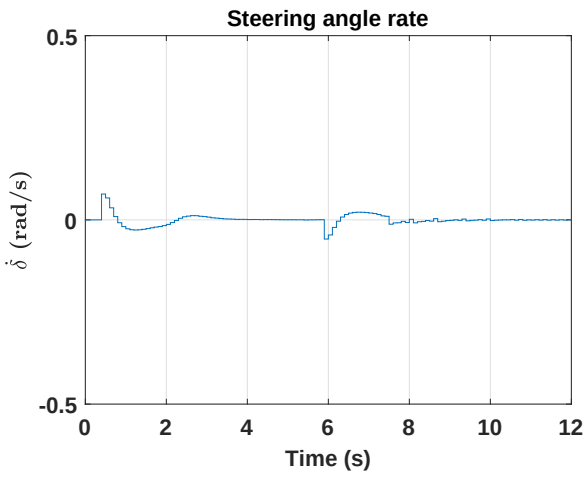

(f) Ego-vehicle steering angle rate $\dot{\delta}$.

Figure 7-11: Ego-vehicle states and control inputs for scenario 4.

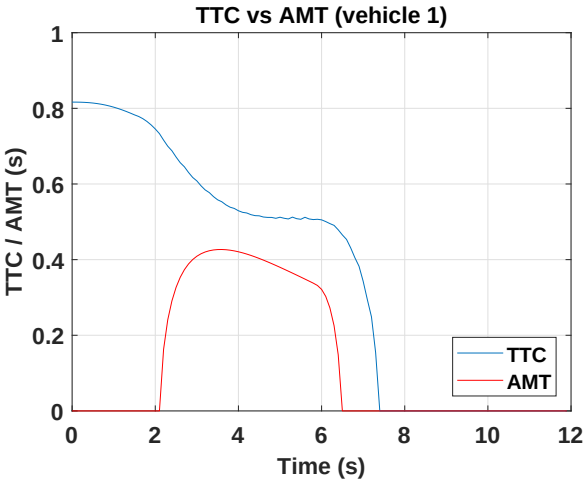

(a) Time-To-Collision and Avoidance-Maneuver-Time for vehicle 1.

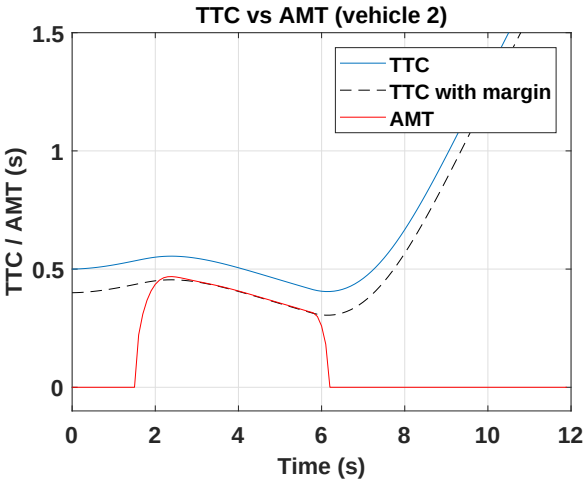

(b) Time-To-Collision and Avoidance-Maneuver-Time for vehicle 2.

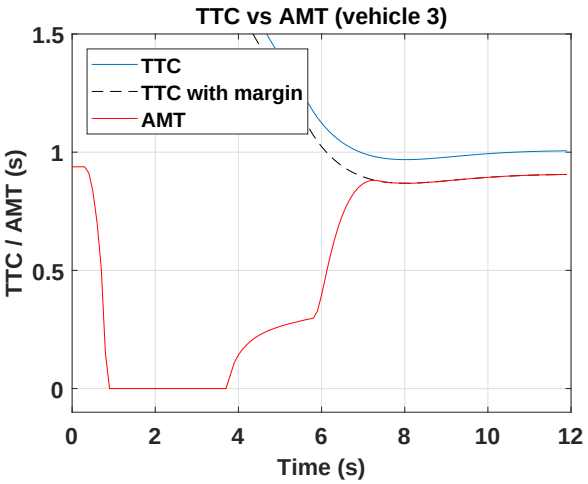

(c) Time-To-Collision and Avoidance-Maneuver-Time for vehicle 3.

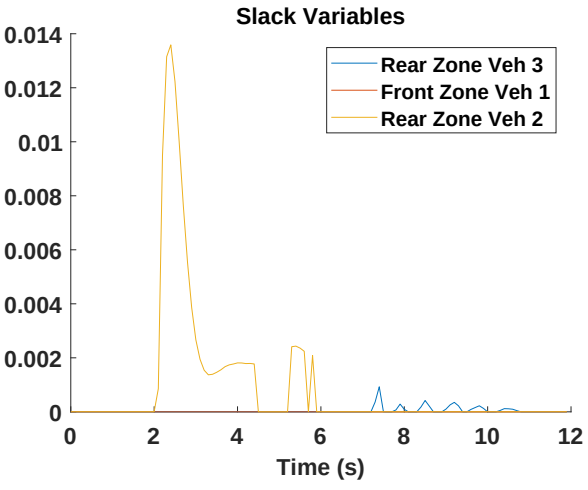

(d) Slack variable values.

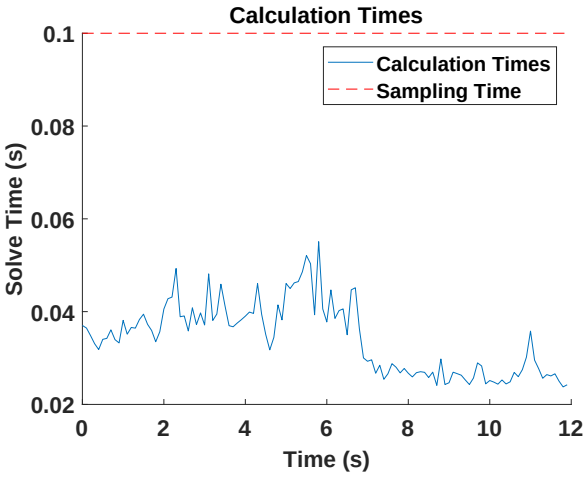

(e) Calculation times and sampling limit.

Figure 7-12: Simulation data for scenario 4.

7-6 Comparison to Earlier Work

As the work in this thesis was proposed by Volvo Cars / Zenuity as a follow-up to an earlier thesis executed under their supervision it is important to evaluate the progress that has been made. To do this the proposed solution by Chandru et al[3] was implemented in the current thesis' simulation environment.

To compare results scenario 1 from Section 7-2 was repeated, and the resulting vehicle movement can be seen in Figures (7-13a) to (7-13g). Although the path planner is able to find the point of maximum lateral intrusion, it shows clearly that without the inclusion of heading into the safety zone the proposed solution will violate the *real* safety constraint, and a prediction in Figure (7-15) shows that the evasion maneuver at for example T=3[s] would actually cause a collision should the leading vehicle come to a stop under worst-case assumptions at that point.

This is also confirmed by the comparison of the Time-To-Collision and the Avoidance-Maneuver-Time in Figure (7-14), as it can be seen the AMT exceeds the TTC between T = 2.5[s] and T = 3.5[s], putting the ego-vehicle at risk in that timeframe.

Further evaluations in previous chapters show that the solution developed in this thesis is able to take into account safety zones on multiple vehicles in multiple lanes. In conclusion, it can be said that the presented work has taken the principles of safe path planning developed in the previous work, and has built on it a control methodology which is safe and usable in realistic scenarios.

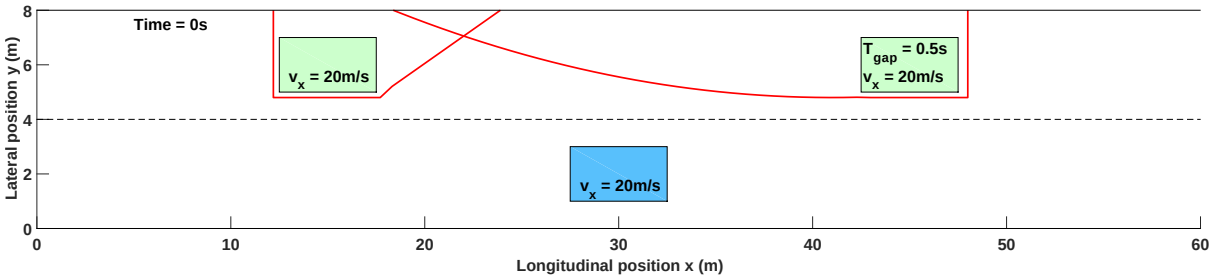

(a) Screen capture at T=0[s].

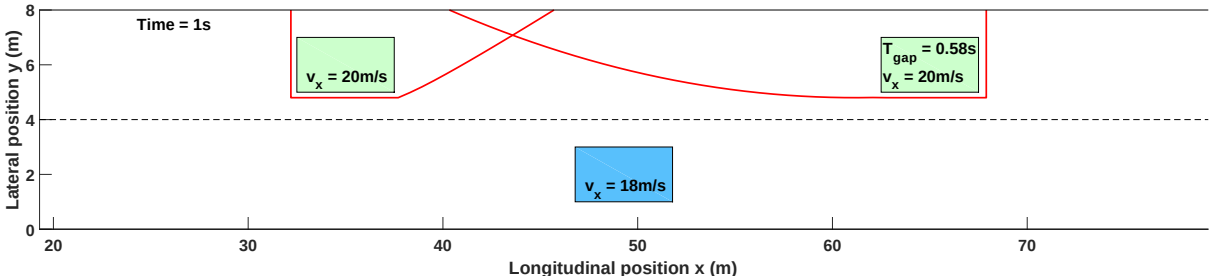

(b) Screen capture at T=1[s].

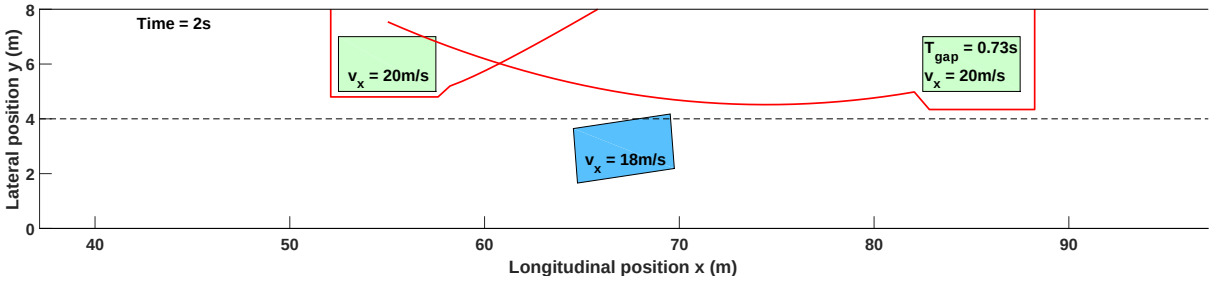

(c) Screen capture at T=2[s].

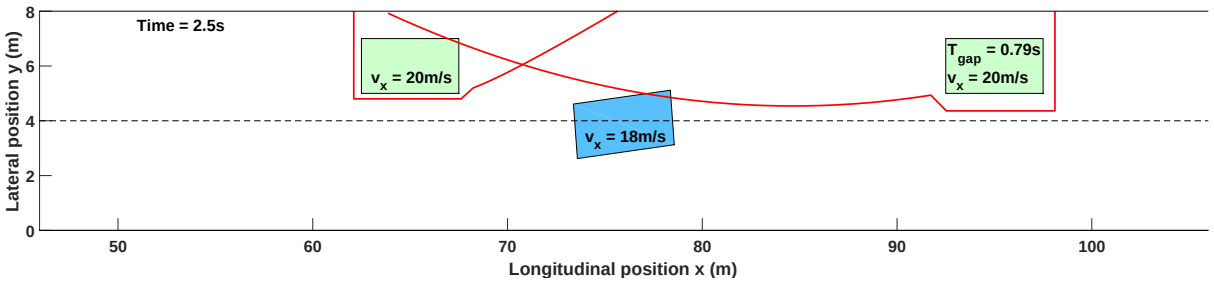

(d) Screen capture at T=2.5[s].

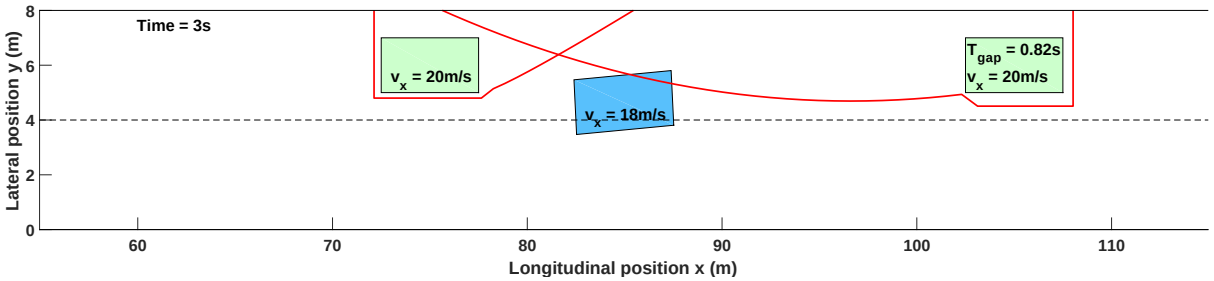

(e) Screen capture at T=3[s].

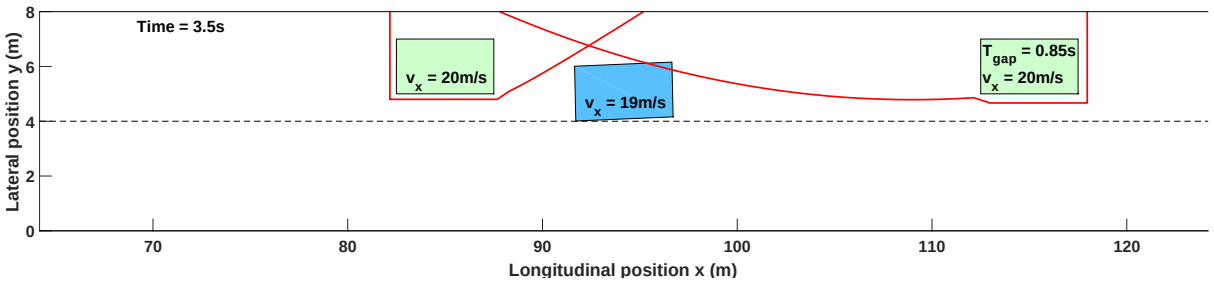

(f) Screen capture at T=3.5[s].

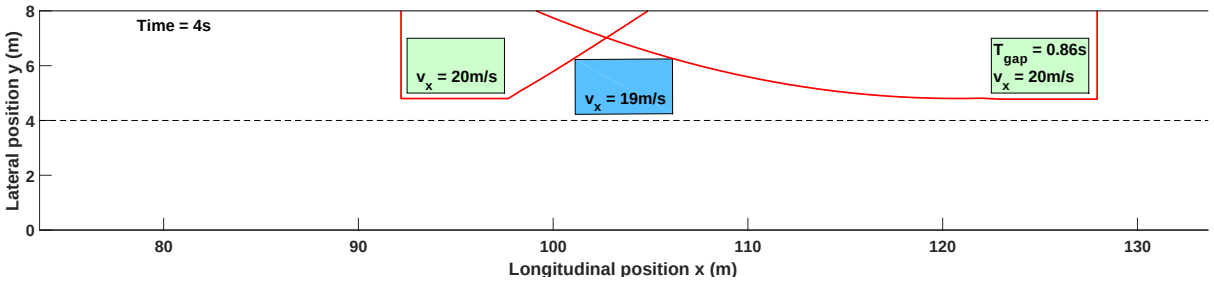

(g) Screen capture at T=4[s].

Figure 7-13: Screen captures of a simulation of scenario 1, using a controller based on the lane change solution proposed by Chandru et al[3], which does not take into account vehicle heading.

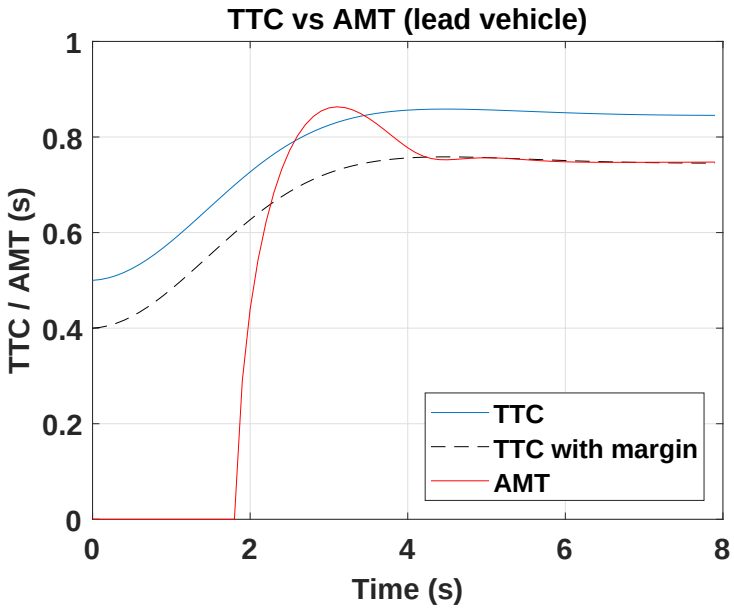

Figure 7-14: Time to Collision and Avoidance Maneuver Time with respect to vehicle 2.

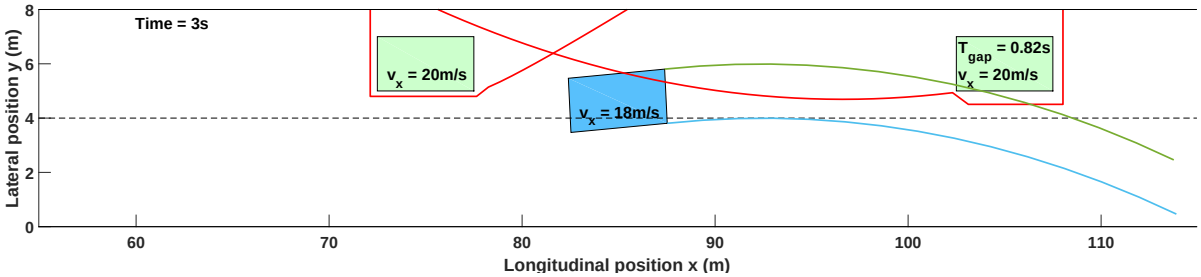

Figure 7-15: Frame capture from the Chandru[3] solution showing the predicted evasion trajectories should the lead vehicle come to an instant stop.

Chapter 8

Conclusion

A commercially available Automated Driving System (level 3 and higher) for highway driving seems to be just around the corner, with many companies introducing (level 2) partial automation systems such as Volvo's Pilot Assist, GM's Super Cruise and Tesla's Autopilot.

Although these systems deal well with ideal driving situations at low traffic density conditions, they struggle to make lane changes when inter-vehicle gaps become smaller. As traffic congestion is only expected to increase in the coming years, this is a problem that urgently needs a solution.

To solve this issue, in this thesis a lane change path planning algorithm was developed that reduces the gap necessary to initiate a lane change between vehicles. This is done without risking the safety of the ADS-operated vehicle by guaranteeing the availability of an evasive maneuver. This allows the Automated Driving System to make *active* lane changes: to initiate a merge by intruding partly into the gap and provoking a reaction from other road users, instead of waiting for them to create a gap.

To guarantee safety, a mathematical safety zone constraint was formulated and a novel 3-step Model Predictive Control scheme was developed to implement it in realistic highway driving scenarios. Solving the three optimisation problems was achieved using the state-of-the-art nonlinear FORCESPro NLP-solver, resulting in fast computation times allowing future real-time implementation.

The summarize, the main scientific conbributions of this thesis are:

- The design a safety zone constraint that guarantees the availability of an evasion maneuver
- The development a method to implement this constraint using the model predictive control framework
- Implementing the control algorithm using a state-of-the-art Interior Point nonlinear solver

In doing this the availability of the lane change maneuver in ADS-operated vehicles is increased, allowing them to maneuver in denser traffic than currently possible, and the introduction of a level 3 Automated Driving System for normal highway driving has been brought one step closer.

8-1 Summary of Conclusions

By looking into path planning methods, in Chapter 2 the conclusion was made that if a mathematical definition for the availability of a back-up maneuver could be made, such a definition

could be implemented using Model Predictive Control. Using this methodology the safety could be guaranteed and the margins reduced.

Analyzing the dynamics of the vehicle and the back-up maneuver in Chapter 3 allowed the adaption of previous theory[3] to create the safety zone in Chapter 4.

Subsequently, in order to implement the designed safety zones on multiple vehicles and to allow overtaking maneuvers within the prediction horizon a framework of three consecutive optimisations was developed and detailed in Chapter 5.

In Chapter 6, the algorithm was implemented using the state-of-the-art ForcesPRO fast nonlinear Interior Point solver, with which average computation times of $\sim$35[ms] were reached on an Intel Core i7 X940 at 2.13[GHz], using a 100[ms] sampling time and a prediction horizon of N = 100 samples. Maximum computation times never exceeded $\sim$ 70[ms], allowing the real-time implementation of the algorithm.

Simulation results in Chapter 7 showed that the designed path planning solution met all requirements and was able to:

1. Change lanes and find the point of maximum lateral intrusion
2. Stay outside the safety zones
3. Plan an evasion maneuver whilst not exceeding the maximum lateral acceleration
4. Take into account safety zones on multiple vehicles, spread over multiple lanes
5. Be robust towards prediction errors on surrounding vehicle behaviour
6. Overtake other vehicles within the prediction horizon

The final comparison shows that the algorithm can guarantee safety as opposed to earlier designs, while now also being able to overtake other vehicles, and handle realistic highway driving scenarios with multiple vehicles spread over multiple lanes.

8-2 Limitations and Future Work

Although the presented work provides a good step in the direction of a highway driving ADS, there are still limitations in the current solution, and the following subsections will try to briefly detail these and provide suggestions for future work following from them.

8-2-1 Lateral Movement by Surrounding Vehicles

The current solution and its safety guarantees are based on the assumption that the surrounding vehicles will only defer from their prediction models in a longitudinal fashion, in other words they will only brake or accelerate unexpectedly, but will not move laterally. It is therefore necessary to abort the ego-vehicle's maneuver once another vehicle decides to, for example, change lane as well. Finding a way to incorporate the lateral movement of surrounding vehicles into the safety zone formulation would be a valuable contribution.

8-2-2 Unpredicted Events and Accidents Analysis

The design of the safety zone is based on a set of 'unpredicted' events and a worst-case scenario of an instant stop. An instant stop is a somewhat unrealistic scenario however, since most accidents involve high to very high decelerations, but not infinite ones. But even though it is unrealistic, it might not even be the real worst case, as a collision with a wrong-way driver might even involve moving backwards. It is therefore necessary to look at a statistical analysis of accidents and decide which scenario's to design for, and which not.

8-2-3 Social Behaviour

As the safety zone toward the trailing vehicle is only based on a cut-off maneuver from behind this results a quite small margin, which, although safe from an ego-vehicle perspective, might be considered rude or even dangerous by the trailing vehicle driver. For the real-life design of a lane change maneuver it is therefore suggested to look not only at the safety of a maneuver, but also to include some metrics on the politeness of a maneuver.

8-2-4 Refinement of Evasion Maneuver Dynamics

In this work the dynamics of the ego-vehicle evasion maneuver are based on a point-mass model. The evasion maneuver could however also be approximated using a steady-state cornering circle. As this would provide a better approximation of the maneuver, the maximum lateral acceleration used to base the safety zone on can lie closer to the real available lateral acceleration (the safety margin can be smaller).

8-2-5 Exploit Simplification of Step 2 and 3 Optimisations

Because of the splitting of the optimisation in 3 steps, the models in step 2 and 3 become Linear Parameter-Varying (LPV)-problems. Because of this there might be computation speed gains by using structure exploited LPV solvers instead of an NLP solver.

8-2-6 Validation on Vehicle Model including Tyre Dynamics

Although the control structure using the MPC-control inputs is assumed to be valid for the nominal driving scenarios as it stays well within the linear regime of the tyre dynamics, the ego-vehicle evasion maneuver might encounter a larger amount of model-mismatch, issuing the necessity to use lower-level controllers to follow the planned state trajectories. It is therefore advised to simulate the evasion scenarios on a higher-order vehicle model.

Bibliography

[1] M. Behrendt, "MPC Scheme. (Own work), distributed under a CC BY-SA 3.0 license," 2009.

[2] J. Nilsson, M. Brannstrom, E. Coelingh, and J. Fredriksson, "Lane Change Maneuvers for Automated Vehicles," *IEEE Transactions on Intelligent Transportation Systems*, vol. PP, no. 99, pp. 1–10, 2016.

[3] R. Chandru and Y. Selvaraj, *Motion Planning for Autonomous Lane Change Manoeuvre with Abort Ability*. Msc thesis, Chalmers University of Technology, 2016.

[4] SAE International, *Taxonomy and Definitions for Terms Related to Driving Automation Systems for On-Road Motor Vehicles*, sep 2016.

[5] N. Kalra and D. G. Groves, "The Enemy of Good: Estimating the Cost of Waiting for Nearly Perfect Automated Vehicles," tech. rep., RAND Corporation, 2017.

[6] C. Berger, *Model Predictive Control Path Planning and state-dependent constraints*. Literature review, Delft University of Technology, 2017.

[7] J. Eriksson and L. Svensson, *Tuning for ride quality in autonomous vehicle*. Msc thesis, Uppsala University, 2015.

[8] C. Katrakazas, M. Quddus, W.-H. Chen, and L. Deka, "Real-time motion planning methods for autonomous on-road driving: State-of-the-art and future research directions," *Transportation Research Part C: Emerging Technologies*, vol. 60, pp. 416–442, 2015.

[9] N. Kalra and S. M. Paddock, "Driving to safety: How many miles of driving would it take to demonstrate autonomous vehicle reliability?," *Transportation Research Part A: Policy and Practice*, vol. 94, pp. 182–193, dec 2016.

[10] M. Brännström, E. Coelingh, J. Sjöberg, M. Brännström, E. Coelingh, and J. Sjöberg, "Decision-making on when to brake and when to steer to avoid a collision," *Int. J. Vehicle Safety J. Vehicle Safety*, vol. 7, no. 1, pp. 87–106, 2014.

[11] M. Werling and D. Liccardo, "Automatic collision avoidance using model-predictive online optimization," in *2012 IEEE 51st IEEE Conference on Decision and Control (CDC)*, pp. 6309–6314, IEEE, dec 2012.

[12] J. Nilsson, Y. Gao, A. Carvalho, and F. Borrelli, "Manoeuvre generation and control for automated highway driving," *IFAC Proceedings Volumes*, vol. 47, no. 3, pp. 6301–6306, 2014.

[13] L. Menhour, B. D'Andréa-Novel, M. Fliess, and H. Mounier, "Coupled nonlinear vehicle control: Flatness-based setting with algebraic estimation techniques," *Control Engineering Practice*, vol. 22, pp. 135–146, 2013.

[14] H. B. Pacejka, *Tyre and vehicle dynamics*. Oxford: Butterworth-Heinemann, 2006.

[15] T. Weiskircher, Q. Wang, and B. Ayalew, "Predictive Guidance and Control Framework for (Semi-)Autonomous Vehicles in Public Traffic," *IEEE Transactions on Control Systems Technology*, pp. 1–13, 2017.

[16] E. C. Kerrigan and J. M. Maciejowski, "Soft Constraints And Exact Penalty Functions In Model Predictive Control," *Control 2000 Conference*, 2000.

[17] S. Gros, M. Zanon, R. Quirynen, A. Bemporad, and M. Diehl, "From linear to nonlinear MPC: bridging the gap via the real-time iteration," *International Journal of Control*, pp. 1–19, 2016.

[18] M. Diehl, H. J. Ferreau, and N. Haverbeke, "Efficient Numerical Methods for Nonlinear MPC and Moving Horizon Estimation Problem Formulation," *Nonlinear model predictive control*, pp. 391–417, 2009.

[19] H. J. Ferreau, C. Kirches, A. Potschka, H. G. Bock, and M. Diehl, "qpOASES: a parametric active-set algorithm for quadratic programming," *Mathematical Programming Computation*, vol. 6, no. 4, pp. 327–363, 2014.

[20] S. Boyd and L. Vandenberghe, *Convex Optimization*. New York, New York, USA: Cambridge University Press, 2004.

[21] T. J. J. Van Den Boom and B. De Schutter, *Optimization in Systems and Control*. Delft: Delft University of Technology, 2015.

[22] A. Zanelli, A. Domahidi, J. Jerez, and M. Morari, "FORCES NLP: an efficient implementation of interior-point methods for multistage nonlinear nonconvex programs," 2017.

[23] J. F. Bard, *Practical Bilevel Optimization*. Springer US, 1 ed., 1998.

[24] S. Shalev-Shwartz, S. Shammah, and A. Shashua, "Safe, Multi-Agent, Reinforcement Learning for Autonomous Driving," *Arxiv*, 2016.

Glossary

List of Acronyms

ACC	Adaptive Cruise Control
LKA	Lane Keeping Aid
ADAS	Advanced Driver Assistance Systems
MPC	Model Predictive Control
SQP	Sequential Quadratic Programming
QP	Quadratic Program
IPM	Interior Point Methods
KKT	Karush-Kuhn-Tucker
NLP	Nonlinear Program
TTC	Time-To-Collision
AMT	Avoidance-Maneuver-Time
RHC	Reciding Horizon Control
OCP	Optimal Control Problem
LPV	Linear Parameter-Varying
NMPC	Nonlinear Model Predictive Control
CM	Centre of Mass
ADS	Automated Driving System